Planar polarization of cilia in the zebrafish floor-plate involves Par3-mediated posterior localization of highly motile basal bodies

Antoine Donati[1], Isabelle Anselme[1], Sylvie Schneider-Maunoury[1*] and Christine Vesque[1*]

[1] Sorbonne Université, CNRS UMR7622, INSERM U1156, Institut de Biologie Paris Seine (IBPS) - Developmental Biology Unit, 75005, Paris, France

*co-senior authors, co-corresponding authors. sylvie.schneider-maunoury@upmc.fr christine.vesque@upmc.fr

Keywords: planar cell polarity, cilium, basal body, zebrafish floor plate, Par3, Vangl2.

Summary statement:

Floor-plate cilia planar polarization is crucial for cerebro-spinal fluid directional flow in zebrafish embryo nervous system. We describe the polarization dynamics and show that it depends on Par3.

ABSTRACT

Epithelial cilia, whether motile or primary, often display an off-centered planar localization within the apical cell surface. This form of planar cell polarity (PCP) involves the asymmetric positioning of the ciliary basal body (BB). Using the mono-ciliated epithelium of the embryonic zebrafish floor-plate, we investigated the

dynamics and mechanisms of BB polarization by live-imaging. BBs were highly motile, making back-and-forth movements along the antero-posterior axis and contacting both the anterior and posterior membranes. Contacts exclusively occurred at junctional Par3 patches and were often preceded by membrane digitations extending towards the BB, suggesting focused cortical pulling forces. Accordingly, BBs and Par3 patches were linked by dynamic microtubules. Later, BBs became less motile and eventually settled at posterior apical junctions enriched in Par3. BB posterior positioning followed Par3 posterior enrichment and was impaired upon Par3 depletion or disorganization of Par3 patches. In the PCP mutant *Vangl2,* BBs were still motile but displayed poorly-oriented membrane contacts that correlated with Par3 patch fragmentation and lateral spreading. We propose an unexpected function for posterior Par3 enrichment in controlling BB positioning downstream of the PCP pathway.

INTRODUCTION

Cilia are conserved microtubule-based organelles nucleated from a modified centriole called the basal body (BB). Motile cilia generate oriented fluid-propelling forces, while primary cilia receive and transduce mechanical and/or chemical signals (Goetz & Anderson, 2010; Wallingford, 2010). To achieve their functions, cilia often display an asymmetric localization within the apical cell surface, a form of planar cell polarity (PCP) called "translational polarity", which involves BB off-centering.

In many vertebrate ciliated tissues such as the mouse cochlea and ependyma, the laterality organ of mouse and zebrafish, and the zebrafish floor-plate (FP), cilium polarity requires PCP proteins such as Van Gogh like 2 (Vangl2), Frizzled (Fz3/6),

Cadherin EGF LAG seven-pass G-type receptors (Celsr1-3) and Dishevelled (Dvl1-3). These proteins localize asymmetrically and are required for proper cilia/BB positioning (Montcouquiol et al., 2003; Borovina et al., 2010; Mirzadeh et al., 2010; Song et al., 2010; Boutin et al., 2012). However, the mechanisms of BB positioning downstream of PCP proteins remain poorly understood. Translational polarity requires non-muscle myosin II in murine ependymal multiciliated cells (Hirota et al., 2010), Rac1 in monociliated cells of the mouse node and cochlea (Grimsley-Myers et al., 2009; Hashimoto et al., 2010) and G protein signalling in mouse cochlear hair cells (Ezan et al., 2013; Tarchini et al., 2013). Some ciliary proteins themselves have also been involved in cilia planar polarization (Ross et al., 2005; Jones et al., 2008; Mirzadeh et al., 2010; Mahuzier et al., 2012; Ohata et al., 2015). However, the link between these different actors and how they impact BB movements is unclear.

Understanding the mechanisms of cilium polarization would highly benefit from a dynamic analysis of BB movements. So far, due to technical limitations, live imaging of cilium polarization has been performed only in cochlear explants where confined Brownian motion of BB was observed (Lepelletier et al., 2013) and in the mouse node (Hashimoto et al., 2010) and ependyma (Hirota et al., 2010) with limited temporal resolution. In this paper we used the zebrafish FP to investigate the dynamics of the polarization process in live embryos. The FP is a simple mono-ciliated epithelium whose posterior-positioned motile cilia propel the embryonic cerebrospinal fluid (Kramer-Zucker et al., 2005; Borovina et al., 2011; Thouvenin et al., 2020).

We show that planar polarization of BBs and their associated cilia is progressive during somitogenesis and is accompanied by a change in the behaviour of the BBs, which are highly motile at early stages and spend an increasing amount of time in contact with the posterior membrane as development proceeds. We found that BBs always contacted membranes at Par3-enriched apical junctions. Par3 became enriched at the posterior apical side of FP cells before BB polarization. Par3 depletion and overexpression of either wild type or dominant-negative forms of Par3 disrupted FP polarization. Furthermore, Par3 distribution along apical junctions was disrupted in a *vangl2* mutant. Thus, we propose that a major role of the PCP pathway in the FP is to drive Par3 asymmetric localization, which in turn mediates BB posterior positioning.

RESULTS

Floor-plate polarization shows temporal progression but no spatial synchronization

Posterior positioning of the BB in the zebrafish FP is visible as soon as 18 hours post-fertilization (hpf) (Mahuzier et al., 2012) and is maintained at least until 72 hpf (Mathewson et al., 2019). From 24 hpf onward, it is instrumental in propelling the cerebrospinal fluid (Borovina et al., 2010; Fame et al., 2016). At late gastrulation stages, ectodermal cell centrioles are already slightly posterior (Sepich et al., 2011).

To define the time-course of FP cell polarization, we assessed BB position along the antero-posterior axis on fixed embryos from the 6s to the 26s stage ("s" stands for "somites") (Fig. 1B, C). We focused all our studies to a single stripe of cells, the

medial FP. For each cell we defined a BB polarization index (p.i. in Fig. 1A). BBs were posteriorly biased at 6s, and the polarization state did not significantly change until 10s. After 10s, there was a progressive increase in polarization, mostly due to an increase in the percentage of cells with a BB in contact with the posterior membrane, with a disappearance of anterior BBs and a reduction of median BBs. The polarization state of the FP did not further increase between 18s and 26s (Fig. 1C). We did not detect any gradient of polarization index along the antero-posterior axis (Fig. S1A), and single non-polarized cells were often intermingled among polarized neighbors (Fig. S1B), arguing against a polarization wave.

BBs are highly motile in FP cells

This static view of BB polarization could reflect very different individual BB behaviours: for instance a slow, regular BB movement towards posterior or a unique fast movement at a specific time point. In order to understand the dynamics of the process, we turned to live-imaging and followed BB movements within the apical surface of individual FP cells at different developmental stages (4s to 21s), using Centrin-GFP to label BBs and mbCherry label membranes. BBs were surprisingly motile within the apical surface (Fig. 2A-D and Movies S1-S4), moving both anteriorly and posteriorly (Fig. S1D, first column and Fig. 6A 'wt'), with a clear BB movement orientation bias along the antero-posterior axis (70% of BB movements) (Fig. 6A, B, wt). At early stages, BBs contacted the anterior and posterior membranes several times per hour (Fig. 6A, B, wt).

Cell deformations along the antero-posterior axis were more important at early stages (4-10 s) (Fig. 2A, B) than at later stages (14-21 s) (Fig. 2C, D), probably due to convergence-extension movements, but many long BB movements did not correlate with cell deformation (see for example the two long movements around 55 and 75 min in Fig. 2A). This suggests that BBs are actively moving within FP cell apical surfaces. One possible explanation for the presence of unpolarized cells is that they had just undergone mitosis. However, mitoses were rare in FP cells at early stages (6 / 79 cells, 9 embryos at 4-8 s) and absent at later stages (118 cells from 15 embryos at 13-21s). Thus, the impact of cell shape changes and mitosis on FP polarization is likely very small.

To sum up, at early polarization stage, BBs actively move along the antero-posterior axis of FP cells and make multiple contacts with anterior and posterior membranes.

FP polarization involves a change in BB behaviour

In order to characterize BB behavioural changes during development, we determined the percentage of time that BBs spent in contact with the posterior membrane (Fig. 2E). At early stages, BBs spent in average 44% of their time in contact with the posterior membrane, versus more than 70% at later stages (13-21s). This was largely due to an increase in the number of cells in which the BB did not detach from the posterior membrane (Fig. 2C). We refer to this situation as “posteriorly docked BB”. At early stages (4-8s), we did not observe any cell with posteriorly docked BB (41 cells, 5 embryos), whereas they made up 34% of the FP cell population at 13-17s stages (13/38 cells, 6 embryos) and almost half (46%) the FP population at later stages (17-21s, 27/59 cells, 7 embryos). We also noted a decrease in the frequency of BB direction changes, as well as an increase in the mean duration of BB/posterior

membrane contact events and mean polarization index, suggesting that, as development proceeds, BB movements become confined posteriorly (Fig. S1D, first line). Posteriorly docked BBs made a significant contribution to these behavioural changes. In order to determine if changes in the behaviour of non-posteriorly docked BBs contributed to the increase of FP polarization during somitogenesis, we quantified the same parameters, but taking-into-account only these motile BBs (Fig. S1D, second line): the same trend in BB behaviour change was observed.

To further characterize the behaviour of non-posteriorly docked BBs, we quantified the frequency of contact events between the BB and either the anterior or the posterior membrane (Fig. 2F and G, respectively). Posterior contacts were more frequent than anterior ones even at 4-8s (compare Fig. 2F and G), confirming that FP cells already had a posterior polarization bias at these early stages. Contacts with the anterior membrane were frequently observed at early stages (50% of BBs made at least one anterior contact per hour, see for example at t=70' in Fig. 2B), but almost never at later stages (3/57 cells). Contact frequency with the posterior membrane was also significantly higher at earlier stages (1.3 contact/h) than at later stages (0.8 contact/h, Fig. 2G). This reduction in the number of contacts could be due to an increase in their duration (Fig. S1D, plot 2nd column, 2nd line) and to a reduction in BB speed. Indeed, we found that BBs moved faster at earlier stages (Fig. S1C, 0.2 µm/min at 4-8 s versus 0.1 µm/min at 13-21 s). Thus, the observed changes in FP polarization are explained both by an increase in the posteriorly docked BB population and by behavioural changes in other BBs.

Digitations of the anterior and posterior apical membranes elongate towards motile BBs

Live-imaging revealed the presence of membrane digitations extending between the BB and anterior or posterior apical membranes (thereafter called ant/post membranes) (Fig. 3; Movies S5 and S6). Digitations always formed at the same apicobasal level as the BB (i.e. around 1 µm under the apical surface). At early stages, in ∆t2min and ∆t5min movies we could detect such digitations in 44% of FP cells (26/59 cells, 9 embryos), most of which were linking the posterior membrane and the BB (83%, 45/54 digitations, Fig. 3A upper row, white arrow, Movie S5), although digitations from the anterior membrane were also seen, with a similar lifetime (Fig. 3A second row, Movie S6, Fig. 3B and C). Posterior digitations (i.e. originating from the posterior membrane) were followed by a posterior directed BB movement in 67% of cases (26/39), whereas anterior digitations were followed by a BB anterior movement in only 22% of cases (2/9) (Fig. 3D). Membrane digitations were rarely seen at later stages (after 14s, 9/40 cells, 10 embryos).

In order to better characterize these digitations, we imaged the floor-plate of wt embryos every 10 seconds (∆t10sec movies, Fig. S2A-C). In these movies, digitations were seen in 80% of FP cells (25/31 cells from 17 embryos). Almost all of them extended from ant/post membranes (92%, 88/95, Fig. S2A) and pointed towards the BB (95%, 90/95 digitations, 25 cells from 14 embryos), while 45% touched the BB. As with our ∆t2min and ∆t5min movies, there was not a good correlation between digitation position (anterior or posterior membrane) and BB movements (Fig. S2C) suggesting that these digitations are a consequence rather than a cause of the forces exerted on BBs.

Dynamic microtubules link BBs and ant/post membranes

Since centrosomes are the main microtubule organizing centers of animal cells and their positioning in many systems depends on microtubules, we investigated microtubule dynamics within the apical surface of FP cells, using GFP-tagged EB3, a microtubule plus end-binding protein. Live-imaging of moving EB3-positive comet-like structures (EB3 comets) revealed highly dynamic microtubules originating from the centrosome/BB and directed to apical junctions (Fig. S2D, Movie S7). The time interval between an EB3 comet coming from the BB touching a spot at the ant/post membrane and the occurrence of either a digitation at this spot or a BB movement towards it was very short: 10 sec in 50% of the cases and less than 1 min in 95% of the cases (Fig. S2E). These observations suggest that the mechanical forces responsible for back-and-forth BB movements are mediated by microtubules.

Overall, our dynamic analysis reveals a highly motile behaviour of BBs in FP cells at early somite stages. As somitogenesis proceeds, BB motility decreases. BBs progressively stop shuttling from anterior to posterior cell junctions and their contacts with the posterior membrane last longer. We also uncover membrane digitations forming at precise spots of ant/post apical membranes and show that these spots are linked to BBs by dynamic microtubules. These results suggest the existence of a molecular complex at precise spots of apical ant/post membranes, which is able to exert mechanical forces on the BB via microtubules, and whose distribution becomes biased to the posterior side of each FP cell during development.

Posterior enrichment of Par3 precedes BB/posterior docking

Par3 (Pard3) is a conserved polarity protein that positions at apical junctions of neuroepithelial cells during zebrafish neurulation and is important for lumen formation (Hong et al., 2010; Buckley et al., 2013). Moreover, Par3 has been shown to modulate centrosome positioning in Drosophila (Inaba et al., 2015; Jiang et al., 2015), making it a good candidate for BB attraction in the zebrafish FP. In order to test this hypothesis, we first assessed Par3 localization by immunostaining (Fig. 4A). At the 14s stage, Par3 localized at apical junctions of FP cells (Fig. 4A). Par3 local enrichments or "patches" were detected on ant/post membranes and in close contact with posteriorly docked BBs (white arrows, Fig. 4A). This distribution was confirmed using a phosphorylated-Par3 antibody ("BazP1085") (Fig. S3A). Par3 patches were also present in FP cells in which the BB was not yet in contact with the posterior membrane (Fig. 4A and S3A right panels) showing that this enrichment precedes stable BB/posterior membrane contact.

In order to test whether Par3 is asymmetrically enriched in FP cells, we mosaically expressed Par3-RFP and centrin-GFP. Quantification of Par3 expression showed that, among fully polarized (p.i. =1) individual Par3-RFP-expressing FP cells, almost all had a Par3-RFP post/ant ratio greater than 1 (Fig. 4B). To determine whether Par3 posterior enrichment preceded BB/posterior docking, we imaged BB movements and quantified Par3-RFP posterior/anterior ratio at each time-point; Par3-RFP was enriched posteriorly before BB/posterior docking (Fig. 4C) (12/14 cells, 12 embryos) (Movie S8). In contrast, BBs of FP cells with weak or no posterior Par3 enrichment remained unpolarized (either making no contact (2/5 cells, 5 embryos) or unstable contacts (3/5 cells, 5 embryos) with the posterior membrane (Fig. 4D and Movie S9).

Thus, Par3 forms patches at FP apical ant/post membranes and BBs dock posteriorly at the level of Par3 patches. In addition, Par3 is enriched posteriorly before BB/posterior membrane contact. Together, this strongly suggests that Par3 is a key player in BB posterior positioning.

BBs contact ant/post membranes exclusively at Par3 patches

During the second half of somitogenesis, Par3 formed a continuous belt at apical junctions of FP cells, although it was locally enriched, forming patches that associated with BBs, as described above. In contrast, at the 4-8s stages, Par3 formed discrete patches at FP apical ant/post membranes, but not at lateral membranes (i.e. apical membranes of medial FP cells in contact with lateral FP cells). These patches were aligned with the antero-posterior axis of the embryo (Fig. 4E, white arrows). Strikingly, BBs/membrane contacts occurred exclusively at these patches (58 cells from 18 embryos) (Fig. 4F and Movies S10 and S11).

In 40% of these cells (23/58), Par3 patches "stretched" towards the BB (Fig. 4F yellow arrows) and were actually covering a membrane digitation (Fig. 4F, t=0' and t=64', Movie S11). 92% of these digitations occurred at a Par3 patch (36/39 digitations from 23 cells and 14 embryos). The presence of membrane digitations and their overlap with Par3 patches point to the existence of mechanical forces between BBs and membranes at Par3 patches and suggests that Par3 could be required for local force generation. This role of Par3 could be more general, since in dividing FP cells, after cytokinesis the centrosomes also always rapidly (within 10min) moved back towards Par3 patches (9/9 cells from 9 embryos, Fig. S3B and Movie S12).

Par3 depletion or altered localization disrupts BB positioning

To test whether Par3 is required for posterior BB positioning in the FP, we analyzed FP polarization in the *MZPard3ab* mutant devoid of maternal and zygotic Pard3ab protein (Blasky et al., 2014). *MZpard3ab*$^{-/-}$ embryos displayed convergence-extension and cell intercalation defects with variable severity. In severely affected embryos (19/55, 34%), these defects precluded the analysis of FP polarity. In mildly affected embryos, in which the medial FP could be unambiguously identified, the BB polarization index was significantly reduced to a moderate extent (Fig. 5A and Fig. S4A). A reduction of BB polarization was also observed in *Mpard3ab*$^{+/-}$ siblings (heterozygotes devoid of maternal Pard3ab, Fig. 5A and Fig. S4A), suggesting that maternal stores of Par3 are important for BB polarization, as confirmed by the strong reduction of Par3 protein level (supplementary Fig. S4C).

In order to obtain further insight into the mechanisms by which Par3 impacts BB positioning, we expressed a dominant-negative form of Par3, Par3Δ6, which localizes less efficiently to apical junctions and more to microtubules (von Trotha et al., 2006) and induces a similar neural ventricle defect as Pard6 gamma mutant (Munson et al., 2008; Buckley et al, 2013). Injection of Par3Δ6-GFP mRNA at the 1 cell-stage led to significant reduction of BB polarization, often accompanied by FP cell intercalation defects along the midline (Fig. 5B and supplementary Fig. S4B). Par3Δ6-GFP was then injected in 1 cell at the 16-32 cell-stage to obtain mosaic expression. In isolated FP cells expressing high Par3Δ6-GFP levels, the BB always colocalized with the most intense GFP patch, either along apical junctions or in the middle of the apical surface (41 cells, 11 embryos) (Fig. 5C). This strongly suggests that Par3Δ6-GFP foci, like wild-type Par3 foci, are able to attract the BB. However, unlike wild-type

Par3, it does not localize efficiently to the posterior apical junctions (17/41) and thus its overexpression perturbs BB polarization.

To confirm that Par3 mis-localization along apical junctions is sufficient to perturb BB polarization, we overexpressed the wild-type form of Par3 (150 pg mRNA per embryo instead of 50 pg in previous injections). As expected, Par3-RFP still localized to FP apical junctions and did not affect apico-basal polarity but significantly disrupted BB posterior positioning (Fig. 5D). Furthermore, Par3-RFP-negative cells adjacent to Par3-RFP over-expressing cells polarized normally, showing that Par3 overexpression effect is cell autonomous (391 cells, 20 embryos, Wilcoxon test p-value=0.19).

These results show that Par3 is necessary for BB posterior positioning in the FP and that it acts by attracting or capturing the BB at posterior apical junctions.

In the PCP mutant *vangl2,* BBs are still motile but make more contacts with lateral membranes

Vangl2, a PCP protein, is involved in zebrafish FP PCP (Borovina et al., 2010) but the mechanisms linking Vangl2 to BB posterior positioning are unknown. We thus analyzed the dynamics of FP polarization in the *vangl2*^{m209} mutant (Solnica-Krezel et al., 1996). At 18s, the BB of *vangl2*$^{m209/m209}$ FP cells was mispositioned at the center of the apical surface, which could suggest either a loss of BB motility or misoriented BB movements (Fig. 7A). Live-imaging of *vangl2*$^{m209/m209}$ FP revealed several BB behaviour changes in *vangl2*$^{m209/m209}$; surprisingly, at early stages in *vangl2*$^{m209/m209}$ FP cells, BBs were still motile and even faster than wt (Fig. 6D). Moreover, BB movements were still biased along the antero-posterior axis (Fig. 6B, 60% of

movements), but BBs made more lateral movements and 10% less antero-posterior movements compared to wt (Fig. 6A and 6B, Movie S13). The length of BB movements, which was smaller in the lateral than in the antero-posterior direction in controls, was equivalent in all directions in *vangl2*$^{m209/m209}$ mutants (Fig. 6A).

Despite the preserved antero-posterior bias in BB movements, *vangl2* mutants showed a striking loss of antero-posterior bias in BB/membrane contacts. The overall proportion of BB movements resulting in BB/membrane contacts was the same as in wt (16% of movements), but the positions of these contacts were very different: in wt, most contacts occurred with the posterior membrane (75%) and almost none with the lateral membranes (3%), whereas in *vangl2*$^{m209/m209}$, BB contacts occurred equally with anterior, posterior or lateral membranes (around 33% each) (Fig. 6D, middle barplot). In addition, *vangl2*$^{m209/m209}$ BBs spent less time in contact with membranes (Fig. 6D, right plot).

At later stages, almost half of the BBs remained in contact with the posterior membrane in wt (Fig. 2E) (posteriorly docked BBs). In *vangl2*$^{m209/m209}$ embryos, the vast majority of BBs did not stably dock at any membrane. Instead, BBs remained at the center of the apical surface. The few BB movements of wt cells as well as the many BB movements seen in *vangl2*$^{m209/m209}$ cells were much smaller than at early stages and had no preferential orientation (Fig. 6A). BB/membrane contacts were half less frequent than at early stages, both in wt and *vangl2*$^{m209/m209}$ but we could still detect a significant difference in their position between wt and *vangl2*$^{m209/m209}$, with more lateral and anterior contacts in *vangl2*$^{m209/m209}$ (Fig. 6E, middle barplot).

In conclusion, in *vangl2* mutants, BBs still show fast, oriented movements along the antero-posterior axis but make aberrant membrane contacts with lateral membranes at early stages, and fail to attach to the posterior membrane at later stages.

BB behaviour defects in *vangl2* mutants are associated with abnormal Par3 clustering and localization

We then wondered if these behavioural defects could be due to Par3 defects. Par3 localized at apical junctions in *vangl2*$^{m209/m209}$, but there was a significant difference in the number and prominence of Par3 patches (prominence: height of Par3 fluorescence peak relative to the highest and nearest local fluorescence minimum, Supplementary Fig. S4D). In wt, 90% of FP cells had at least a major Par3 patch (Fig. 7B, yellow arrows), with 39% of cells also having smaller secondary patches (Fig. 7C), while in *vangl2*$^{m209/m209}$ embryos, the number of FP cells with at least one Par3 patch was unchanged (around 90% of cells) but the number of cells with more than one patch was increased (54% of cells). In addition, the prominence of Par3 patches was decreased in *vangl2*$^{m209/m209}$ embryos (Fig. 7D). Thus, Par3 forms more numerous, smaller patches in *vangl2* mutants, showing a role for Vangl2 in Par3 clustering.

To further analyze a potential link between abnormal BB behaviour and Par3 patches mis-localization in *vangl2*$^{m209/m209}$ embryos, we made time-lapse movies of mutant embryos mosaically injected with Par3-RFP (7 embryos, 17 cells, see two examples in Fig. 7F and Movies S13 and S14). In *vangl2* mutants, BBs still contacted the membrane only at Par3 patches (Fig. 7F), suggesting that Vangl2 did not directly affect the ability of Par3 patches to attract BBs. However, the distribution of Par3 patches was very different. Early *vangl2*$^{m209/m209}$ embryos displayed more cells with lateral Par3 patches compared to wt (70% vs 20%, Fig. 7E). In addition, they had more cells with an anterior Par3 patch (82% vs 67%) and less cells with a posterior patch (65% vs 87%).

These results strongly suggest that, in *vangl2*$^{m209/m209}$ embryos, abnormal BB behaviour and polarization failure are due to the fragmentation and mispositioning of Par3 patches along the apical junctions of FP cells.

DISCUSSION

In this paper we have analyzed the dynamics of BB posterior positioning in the embryonic zebrafish FP. We show that, during early somitogenesis, BBs are highly motile and able to contact apical junctions several times per hour. As somitogenesis proceeds, BBs settle down posteriorly at junctions enriched in Par3, and we show that Par3 enrichment is essential for BB posterior localization. In the PCP mutant *vangl2*, BBs poorly oriented movements correlate with Par3 patches fragmentation and lateral spreading (Fig. 8). This leads us to propose a model in which Par3 posterior enrichment, downstream of the PCP pathway, increases BB attraction forces from the posterior side, which eventually results in its docking at the posterior Par3 patch (Fig. 8).

BBs exhibit high motility in FP cells of wt and vangl2 mutant embryos

Our live-imaging studies revealed that BBs make rapid back and forth movements within the FP cell apical surface. This contrasts with the mouse cochlear hair cells, where live-imaging of explants at a higher time scale have suggested very slow (10-50 nm/h) and regular BBs movements to the lateral cortex (Lepelletier et al., 2013). Our live imaging also uncovered a clear antero-posterior bias in BB movements, indicating that the orientation of the forces underlying these movements is biased along the polarization axis from early stages on. It will be interesting to investigate

whether this high motility of the BB is conserved in other tissues undergoing cilia translational polarity. Strikingly, live-imaging revealed that in *vangl2*$^{m209/m209}$ embryos, BBs are still highly motile. Major differences with wt BBs are that they make many contacts with lateral membranes and that their contacts are shorter. This suggests that there are cues at the membrane organizing/driving BB movements, and that these cues are disorganized in PCP mutants.

Reciprocal relationships between the cilium and its Par3-mediated planar polarity

FP polarization is concomitant with cilia growth and most BBs are already off-centered at mid-somitogenesis (Fig. 1), suggesting that a fully-grown cilium is not required for the process. This is in line with the observation that the *MZoval/ift88* zebrafish mutant, devoid of cilia, displays correct BB planar polarity (Borovina et al., 2013). The polarization process ends before lumen opening (24 hpf), which also excludes a function of cilia-mediated directional fluid flow as a mechanical instructive cue, as shown in ependymal cells (Guirao et al., 2010). However, several proteins of the cilium base are required for PCP, in the zebrafish FP or in the cochlea (Jones et al., 2007; Mahuzier et al., 2012; May-Simera et al., 2015). This may be explained by the ability of these proteins to modulate PCP protein stability and/or sub-cellular localisation, as shown for Rpgrip1l on Dishevelled (Mahuzier et al., 2012) or BBS8 and Ift20 on Vangl2 (May-Simera et al., 2015), or by microtubule-nucleating functions at BB sub-distal appendages (Kodani et al., 2013).

The high motility of the BBs was unexpected, given that they anchor a growing cilium to the membrane. A possibility is that the growing cilium is still internal at early stages and only protrudes outside when anchored to the posterior junction belt. Such inside cilia have been described recently in other systems (Hong et al., 2010, Insinna et al., 2019; Matsumoto et al., 2019). Alternatively, fluidity of the apical membrane may allow these ciliary movements before the appearance of the tight junction belt and the apical cortical actin meshwork at neural rod stage (Ciruna et al., 2006). Finally, ciliary TZ and BB rootlet maturation may not be complete while cilia are still growing. Such adhesion/anchoring role for TZ proteins have been described in C. Elegans (Schouteden et al., 2015).

Another open question is how Par3-mediated BB polarity impacts the function of ciliated tissues. BB posterior positioning could allow coordinating cell intrinsic PCP with tissue polarity. In the mouse node, it has been proposed that membrane bending at the level of apical junctions facilitates oriented cilia tilting and beating (Hashimoto et al., 2010). Such membrane bending has not been documented in zebrafish. However, in *MZvangl2*$^{-/-}$ embryos in which BBs remain at the center of the apical surface, ciliary beating is not properly oriented (Borovina et al., 2010), which suggests that BB posterior position favors posterior tilting of motile cilia through unknown mechanisms.

Par3 cortical patches recruit the BB.

We proposed the asymmetric maturation of cell junctions as a possible cause for posterior BB positioning. Accordingly, Par3 accumulated in patches at the posterior apical junctions of FP cells before BB posterior docking, and perturbation of Par3 localization affected BB polarization. Interestingly, in the Drosophila early gastrula

ectoderm, aPKC loss-of-function leads to Par3 accumulation as discrete patches that recruit centrosomes (Jiang et al., 2015). Centrosome docking at Par3 patches has also been observed in Drosophila germ stem cells and is critical for oriented division (Inaba et al., 2015). Together with these published data, our results strongly suggest that Par3 may be broadly involved in recruitment of centrosomes/BBs in different systems.

Our live-imaging data strongly suggest that Par3 is involved in generating mechanical forces on the BB to pull it toward the membrane. First, BB/membrane contacts occur exclusively at Par3 patches. Second, membrane digitations support the existence of mechanical forces between Par3 patches and BBs. Third, the predominance of posterior digitations over anterior ones (Fig. 3B) suggests that more force is exerted on the BB from the posterior side, where Par3 is enriched. Such membrane digitations have been previously observed during cell division in the *C. elegans* zygote (Redemann et al., 2010), in the *C. intestinalis* embryo ectoderm (Negishi et al., 2016) and in rare cases at the immunological synapse (Yi et al., 2013). In all cases, the existence of pulling forces between the centrosome and the membrane has been proposed.

We propose that digitations are a consequence of mechanical forces between the BB and Par3 patches rather than a driver of BB movement. First, even in Δt10sec movies, only half of BB movements were associated with digitations and second, there was not a good correlation between the location of a digitation and the direction of BB movement. One can wonder why digitation formation occurs for some BB movements and not others. A possibility is that digitation formation depends both on mechanical forces pulling the membrane and on cortical stiffness.

Possible role of microtubules in BB recruitment to Par3 patches

Our results suggest that mechanical forces between Par3 and the BB could be exerted by microtubules. Dynamic microtubules link the BB and Par3 patches before BB movements and/or digitation formation. Microtubules are required for digitation formation in several systems (Redemann et al., 2010; Negishi et al., 2016) and are thus likely to transmit mechanical forces between BB and Par3 patches that lead to BB movements and/or membrane digitations.

An interesting further question concerns the mechanisms that regulate microtubule dynamics to lead to BB movements. BB movements towards Par3 patches could involve local microtubule depolymerization at the patch, coupled to microtubule anchoring by dynein as proposed for the immunological synapse ("end-on-capture-shrinkage" mechanism) (Yi et al., 2013). Indeed, Par3 can interact with Dynein (Schmoranzer et al., 2009) and with microtubules, directly (Chen et al., 2013) or indirectly (Benton and St Johnston, 2003). Consistent with a role for cortical dynein, a recent study in mouse ependymal cells showed a role of cortical dynein in the off-centering of BB clusters (Takagishi et al., 2020). Moreover, dynein cortical localization depends on Daple, which is a known partner of Par3.

Par3 could also regulate microtubule depolymerization via Rac1, which mediates Par3 function in the mouse cochlea (Landin Malt et al., 2019). In different systems, Par3 regulates the local activity of Rac via the RacGEFs Tiam1 and Trio (Nishimura et al., 2005; Zhang and Macara, 2006; Matsuzawa et al., 2016). Par3 can increase microtubule catastrophe rate by inhibiting Trio in neural crest cells (Moore et al., 2013), and Rac1 can regulate microtubule dynamics via CLIP-170 or Stathmin in other systems (Fukata et al., 2002; Wittmann et al., 2004).

Interestingly, microtubules also actively maintain BB polarity at later stages in the FP, but whether microtubules act as mechanical forces generators or as tracks for PCP proteins transport and asymmetric localization is unknown: indeed, Vangl2 asymmetric localization depends on microtubules (Mathewson et al., 2019). This role of microtubules in PCP protein localization appears widely conserved (Shimada et al., 2006; Vladar et al., 2012). Furthermore, Par3 apical localization also depends on microtubules in zebrafish embryo neural tube (Buckley et al., 2013). Thus, it might prove difficult to disentangle the different roles of microtubules in the asymmetric positioning of BBs of FP cells.

The core PCP protein Vangl2 is involved in BB positioning via Par3 enrichment to the posterior membrane

Our results on *vangl2* mutants lead us to propose that the role of PCP in BB posterior docking is, at least in part, mediated by Par3 localization (Fig.8). How PCP proteins act on Par3 localization in the FP remains to be uncovered. In FP cells, Vangl2 localizes anteriorly (Davey et al., 2016); thus, Vangl2 effect on Par3 could be mediated by Dvl. Indeed, Vangl2 is required for asymmetric localization of Dvl in planar polarized tissues and Dvl can recruit Par3 to the posterior membrane in Drosophila sensory organ precursors (Banerjee et al., 2017). Dvl could also recruit Par3 via Daple, which colocalizes with Par3 in the mouse cochlea and can bind Dvl and Par3 in yeast two-hybrid assays (Siletti et al., 2017). Recent studies have shown that Par3 is planar polarized in several systems, like Drosophila ommatidia (Aigouy and Le Bivic, 2016) and sensory organ precursors (Besson et al., 2015), Xenopus embryo ectoderm (Chuykin et al., 2018) and mouse cochlea (Landin Malt et al.,

2019), suggesting that in addition to its classical role in apico-basal polarization, Par3 might also be involved in PCP across species.

Finally, as asymmetric centriole positioning is now recognized as a conserved PCP readout (Carvajal-Gonzalez et al., 2016a; 2016b), it will be interesting to investigate whether Par3 has a conserved role in centriole/BB positioning in other species where BB/centriole off-centering has been described and also depends on PCP proteins, for example in the embryo of Clytia *hemisphaerica* (Momose et al., 2012) or in Drosophila pupal wing (Carvajal-Gonzalez et al., 2016b).

MATERIALS AND METHODS

Zebrafish handling and experimentation

Wild-type and mutant zebrafish embryos were obtained by natural spawning. We used wild-type AB or (TL x AB) hybrid strains, *vangl2*^{m209} mutants (Solnica-Krezel et al., 1996), ZDB-GENO-190204-5) and *pard3ab*^{fh305} mutants (Blasky et al., 2014), ZDB-FISH-150901-20689). To produce embryos lacking maternal stores of Pard3ab protein, *pard3ab*$^{-/-}$ females were crossed with *pard3ab*$^{+/-}$ males, which led to 50% *MZPard3ab*$^{-/-}$ and 50% *MPard3ab*$^{+/-}$ offspring. To obtain the early stages (4-8s), embryos were collected at 10 am and incubated for 9 h in a 33°C incubator. To obtain later stages (14-20s), embryos were collected at 10 am and incubated for 2 h at 28 °C before being placed overnight in a 24 °C incubator. All our experiments were made in agreement with the European Directive 210/63/EU on the protection of animals used for scientific purposes, and the French application decree ‘Décret 2013-118’. The projects of our group have been approved by our local ethical

committee ‘Comité d'éthique Charles Darwin’. The authorization number is 2015051912122771 v7 (APAFIS#957). The fish facility has been approved by the French ‘Service for animal protection and health’ with approval number A-75-05-25.

mRNA injection

mRNAs were synthesized from linearized pCS2 vectors using the mMESSAGE mMACHINE SP6 transcription kit (Ambion). The following amounts of mRNA were injected: 22 pg for Centrin-GFP, 40 pg for mbCherry (membrane Cherry) or Membrane-GFP (Gap43-GFP), 50 pg for EB3-GFP, 50 pg for Par3-RFP live-imaging, 150pg Par3-RFP for over-expression experiments, 60 pg for Par3Δ6-GFP. mRNAs were injected at the one cell stage for whole embryo expression and at the 16-32 cell stage in a single blastomere for mosaic expression.

Immunostaining

For immunostaining, embryos were fixed in Dent fixative (80% Methanol, 20% DMSO) at 25°C for 2 h, blocked in 5% goat serum, 1% bovine serum albumin and 0.3% triton in PBS for 1 h at room temperature and incubated overnight at 4 °C with primary antibodies and 2 h at room temperature with secondary antibodies. The yolk was then removed and the embryo mounted dorsal side up in Vectashield medium on a slide. Imaging was done using a Leica TCS SP5 AOBS upright confocal microscope using a 63X oil lens. A list of antibodies is given in the supplementary methods.

Live imaging

Embryos were dechorionated manually and mounted in 0.5% low-melting agarose in E3 medium. Movies were recorded at the temperature of the imaging facility room (22 °C) on a Leica TCS SP5 AOBS upright confocal microscope using a 63X (NA 0.9) water immersion lens. The embryos were mounted either with dorsal side up (for early stages or after 18s, when FP cells apical surface is quite large) or on the side (for most 13-18s embryos, when the apical surface of FP cells is narrower and when the images are more blurred when taken from a dorsal view, maybe because of the thickness of the overlying neural tube). The anterior side of the embryos was positioned on the left and their antero-posterior axis aligned horizontally. A z-stack was acquired every 2 or 5min (or in some rarer cases every 4min) for most analysis (Δt2min and Δt5min movies) and every 10sec for some movies (digitations analysis and microtubule dynamics in Fig.S2, Δt10sec) with a z-step of 0.3µm. For each time-point the z-stack extended from the most dorsal side of the notochord to neural cells above the FP for Δt2min and Δt5min movies but was narrower for Δt10sec movies (to allow fast acquisition and reduce photobleaching and photodamage). For embryos mounted on the side, the z-stack extended through all the width of the FP. In every case, the z-stack encompassed FP cells apical surface with the moving BBs. For each time-point we then made a z-projection from a 3µm thick substack that encompass the apical centrioles/BB.

Quantification and statistical analysis

All bar-plots, boxplot and violin plots and statistical tests (as indicated in figure legends) were generated with R (version 3.3.2) and Rstudio (Version 1.1.463). ns (non-significant): $p>0.05$, *: $p<0.05$, **: $p<0.01$, ***: $p<0.001$, ****: $p<0.0001$.

BB position and movements

In all our images, the antero-posterior axis (easily visualized thanks to the underlying notochord, whose cells have an elongated shape orthogonal to the antero-posterior axis) is horizontal and the anterior side of the embryo is toward the left. To assess the polarization of FP cells, we used FIJI to first make a z-projection of thickness 3µm around the centrioles. We then manually measured the distance "a" by drawing a line between the most posterior centriole and the posterior membrane that was parallel to the antero-posterior axis of the embryo (ie parallel to the horizontal axis of the image) and the distance "b" by drawing a similar line, at the same level and also parallel to the antero-posterior axis, between the anterior and posterior membrane (Fig. 1A, dorsal view). We used a similar method for embryos mounted on the side (Fig. 1A lateral view). The polarization index (p.i.) was then calculated as 1-(a/b). In some rare cases, the ant/post membranes in our z-projection around the centrioles are blurry (Fig.2b); in these cases however, going slightly more basally through the z-stack allows us to see a sharper membrane which is usually located just beneath the boundary of the above blurry region.

To follow the evolution of polarization index, the distances "a" and "b" were measured manually at each time-frame in FIJI. These distances and the polarization index were then plotted using python matplotlib (Python 2.7.13) and analyzed with a custom python script to extract relevant information such as the frequency of contact with posterior membrane or percentage of total time spent in contact with posterior membrane. (Fig. 2 and Fig. S1).

For automatic tracking of BB movements (Fig. 5), BB were tracked using Image J TrackMate (Tinevez et al., 2017). The movements were then manually curated to only keep active BB movements and not BB movements due to global shift of cells (especially at early stages when convergence-extension movements are still important), and to indicate whether a contact with an anterior, posterior or lateral membrane occurred. The results were then processed using a custom python script to calculate each movement length and angle relative to the horizontal axis (ie the antero-posterior axis of the embryo) and plotted using Python Matplotlib and R ggplot2. We defined antero-posterior movements as the ones with angles relative to horizontal axis inferior to 45° (ie in the intervals [315-45°[and [135-225°[in Fig. 6A).

For all analyzes, lateral membranes are defined as the ones more parallel to the horizontal axis and ant/post membranes as the ones more orthogonal to the horizontal axis. The transition between lateral and ant/post membranes is evidenced by "Y"-shaped tri-cellular junctions (as in Fig. 4A) or sharp turns in the membrane (as in Fig. 7F).

Par3-RFP posterior to anterior ratio

Fluorescence intensity was measured along the anterior-posterior length of isolated labelled FP cells in FIJI. A custom python script was then used to extract the first quarter (cell anterior side) and last quarter (cell posterior side) of fluorescence intensity values, to determine the area under each curve (corresponding to fluorescence intensity), calculate the post/ant ratio and plot it along with the polarization index (see BB movements analysis section).

Par3 peaks quantification

Fluorescence intensity from immunostained embryos was measured along ant/post membranes of medial FP cells and exported to Matlab (R2018a). For each cell, the "findpeaks" function was used to detect Par3 fluorescence peaks and measure their prominence (Fig. S4D), which was then normalized by the minimal Par3 fluorescence value along the junction.

Additional softwares

Adobe Photoshop was used to assemble the figures. Fig. 1A was done in Microsoft Powerpoint and Fig. 8 with Adobe Illustrator.

Antibodies and plasmids: see supplementary information

ACKNOWLEDGEMENTS

We are grateful to the aquatic animal and cell imaging facilities of the Institut de Biologie Paris-Seine (FR3631, Sorbonne Université, CNRS, Paris, France) for their assistance. We thank Teresa Ferraro for helping with image analysis, Marie Breau for live imaging advice, Alexis Eschstruth for technical assistance and Sophie Gournet for helping with Fig. 8. We thank Paula Alexandre for the kind gift of pCS2-Par3-RFP, Jon Clarke for pCS2-Par3Δ6-GFP, Andreas Wodarz for the BazP1085 antibody, Maximilien Furthauer for the *vangl2*^{m209} line. We thank Nicolas David, Marie Breau and Pierre-Luc Bardet for critical reading and insightful comments on the manuscript. This work was supported by funding from the Agence Nationale pour la Recherche (ANR, project CILIAINTHEBRAIN to SSM) and the Fondation pour la Recherche Médicale (Equipe FRM DEQ20140329544 and EQU201903007943 funding to SSM)**.** A.D was supported by fellowships from the Ecole Normale Supérieure de Cachan and from the Fondation ARC contre le Cancer. The authors declare no competing financial interests.

REFERENCES

Aigouy, B., Le Bivic, A., 2016. The PCP pathway regulates Baz planar distribution in epithelial cells. Sci. Rep. 6, 33420.

Akhmanova, A., Stehbens, S.J., Yap, A.S., 2009. Touch, Grasp, Deliver and Control: Functional Cross-Talk Between Microtubules and Cell Adhesions. Traffic 10, 268–274.

Alexandre, P., Reugels, A.M., Barker, D., Blanc, E., Clarke, J.D.W., 2010. Neurons derive from the more apical daughter in asymmetric divisions in the zebrafish neural tube. Nat. Neurosci. 13, 673–679.

Banerjee, J.J., Aerne, B.L., Holder, M.V., Hauri, S., Gstaiger, M., Tapon, N., 2017. Meru couples planar cell polarity with apical-basal polarity during asymmetric cell division. eLife 6.

Benton, R., St Johnston, D., 2003. Drosophila PAR-1 and 14-3-3 inhibit Bazooka/PAR-3 to establish complementary cortical domains in polarized cells. Cell 115, 691–704.

Besson, C., Bernard, F., Corson, F., Rouault, H., Reynaud, E., Keder, A., Mazouni, K., Schweisguth, F., 2015. Planar Cell Polarity Breaks the Symmetry of PAR Protein Distribution prior to Mitosis in Drosophila Sensory Organ Precursor Cells. Curr. Biol. 25, 1104–1110.

Blasky, A.J., Pan, L., Moens, C.B., Appel, B., 2014. Pard3 regulates contact between neural crest cells and the timing of Schwann cell differentiation but is not essential for neural crest migration or myelination: PARD3 IN NC MIGRATION AND SCHWANN CELL MYELINATION. Dev. Dyn. 243, 1511–1523.

Borovina, A., Superina, S., Voskas, D., Ciruna, B., 2010. Vangl2 directs the posterior tilting and asymmetric localization of motile primary cilia. Nat. Cell Biol. 12, 407–412.

Borovina, A., Ciruna, B. 2013. IFT88 plays a cilia- and PCP-independent role in controlling oriented cell divisions during vertebrate embryonic development. Cell Rep. 5(1):37-43.

Boutin, C., Goffinet, A.M., Tissir, F., 2012. Chapter Seven - Celsr1–3 Cadherins in PCP and Brain Development. In: Yang, Y. (Ed.), Current Topics in Developmental Biology, Planar Cell Polarity During Development. Academic Press, pp. 161–183.

Buckley, C.E., Ren, X., Ward, L.C., Girdler, G.C., Araya, C., Green, M.J., Clark, B.S., Link, B.A., Clarke, J.D.W., 2013. Mirror-symmetric microtubule assembly and cell interactions drive lumen formation in the zebrafish neural rod. EMBO J. 32, 30–44.

Carvajal-Gonzalez, J.M., Mulero-Navarro, S., Mlodzik, M., 2016a. Centriole positioning in epithelial cells and its intimate relationship with planar cell polarity. BioEssays 38, 1234–1245.

Carvajal-Gonzalez, J.M., Roman, A.-C., Mlodzik, M., 2016b. Positioning of centrioles is a conserved readout of Frizzled planar cell polarity signalling. Nat. Commun. 7, 11135.

Chen, S., Chen, J., Shi, H., Wei, M., Castaneda-Castellanos, D.R., Bultje, R.S., Pei, X., Kriegstein, A.R., Zhang, M., Shi, S.-H., 2013. Regulation of Microtubule Stability and Organization by Mammalian Par3 in Specifying Neuronal Polarity. Dev. Cell 24, 26–40.

Chuykin, I., Ossipova, O., Sokol, S.Y., 2018. Par3 interacts with Prickle3 to generate apical PCP complexes in the vertebrate neural plate. eLife 7, e37881.

Ciruna, B., Jenny, A., Lee, D., Mlodzik, M., Schier, A.F. 2006. Planar cell polarity signalling couples cell division and morphogenesis during neurulation. Nature 439(7073):220-4.

Davey, C.F., Mathewson, A.W., Moens, C.B., 2016. PCP Signaling between Migrating Neurons and their Planar-Polarized Neuroepithelial Environment Controls Filopodial Dynamics and Directional Migration. PLOS Genet. 12, e1005934.

Distel, M., Wullimann, M.F., Köster, R.W., 2009. Optimized Gal4 genetics for permanent gene expression mapping in zebrafish. Proc. Natl. Acad. Sci. 106, 13365–13370.

Ezan, J., Lasvaux, L., Gezer, A., Novakovic, A., May-Simera, H., Belotti, E., Lhoumeau, A.-C., Birnbaumer, L., Beer-Hammer, S., Borg, J.-P., Le Bivic, A., Nürnberg, B., Sans, N., Montcouquiol, M., 2013. Primary cilium migration depends on G-protein signalling control of subapical cytoskeleton. Nat. Cell Biol. 15, 1107–1115.

Fame, R.M., Chang, J.T., Hong, A., Aponte-Santiago, N.A., Sive, H., 2016. Directional cerebrospinal fluid movement between brain ventricles in larval zebrafish. Fluids Barriers CNS 13.

Fukata, M., Watanabe, T., Noritake, J., Nakagawa, M., Yamaga, M., Kuroda, S., Matsuura, Y., Iwamatsu, A., Perez, F., Kaibuchi, K., 2002. Rac1 and Cdc42 capture microtubules through IQGAP1 and CLIP-170. Cell 109, 873–885.

Goetz, S.C., Anderson, K.V. 2010. The primary cilium: a signalling centre during vertebrate development. Nat Rev Genet. 11(5):331-44.

Grimsley-Myers, C.M., Sipe, C.W., Geleoc, G.S.G., Lu, X., 2009. The Small GTPase Rac1 Regulates Auditory Hair Cell Morphogenesis. J. Neurosci. 29, 15859–15869.

Guirao, B., Meunier, A., Mortaud, S., Aguilar, A., Corsi, J.M., Strehl, L., Hirota, Y., Desoeuvre, A., Boutin, C., Han, Y.G., Mirzadeh, Z., Cremer, H., Montcouquiol, M., Sawamoto, K., Spassky, N. 2010. Coupling between hydrodynamic forces and planar cell polarity orients mammalian motile cilia. Nat Cell Biol. 12(4):341-50.

Hanovice, N.J., McMains, E., Gross, J.M., 2016. A GAL4-inducible transgenic tool kit for the in vivo modulation of Rho GTPase activity in zebrafish: Modulating Rho GTPase Activity in zebrafish. Dev. Dyn. 245, 844–853.

Hashimoto, M., Shinohara, K., Wang, J., Ikeuchi, S., Yoshiba, S., Meno, C., Nonaka, S., Takada, S., Hatta, K., Wynshaw-Boris, A., Hamada, H., 2010. Planar polarization of node cells determines the rotational axis of node cilia. Nat. Cell Biol. 12, 170–176.

Hegan, P.S., Ostertag, E., Geurts, A.M., Mooseker, M.S., 2015. Myosin Id is required for planar cell polarity in ciliated tracheal and ependymal epithelial cells. Cytoskeleton 72, 503–516.

Hirota, Y., Meunier, A., Huang, S., Shimozawa, T., Yamada, O., Kida, Y.S., Inoue, M., Ito, T., Kato, H., Sakaguchi, M., Sunabori, T., Nakaya, M. -a., Nonaka, S., Ogura, T., Higuchi, H., Okano, H., Spassky, N., Sawamoto, K., 2010. Planar polarity of multiciliated ependymal cells involves the anterior migration of basal bodies regulated by non-muscle myosin II. Development 137, 3037–3046.

Hong, E., Jayachandran, P., Brewster, R. 2010. The polarity protein Pard3 is required for centrosome positioning during neurulation. Dev Biol. 341(2):335-45.

Inaba, M., Venkei, Z.G., Yamashita, Y.M., 2015. The polarity protein Baz forms a platform for the centrosome orientation during asymmetric stem cell division in the Drosophila male germline. Elife 4, e04960.

Insinna, C., Lu, Q., Teixeira, I., Harned, A., Semler, E.M., Stauffer, J., Magidson, V., Tiwari, A., Kenworthy, A.K., Narayan, K., Westlake, C.J. 2019. Investigation of F-BAR domain PACSIN proteins uncovers membrane tubulation function in cilia assembly and transport. Nat Commun. 10(1):428.

Jiang, T., McKinley, R.F.A., McGill, M.A., Angers, S., Harris, T.J.C., 2015. A Par-1-Par-3-Centrosome Cell Polarity Pathway and Its Tuning for Isotropic Cell Adhesion. Curr. Biol. 25, 2701–2708.

Jones, C., Roper, V.C., Foucher, I., Qian, D., Banizs, B., Petit, C., Yoder, B.K., Chen, P., 2008. Ciliary proteins link basal body polarization to planar cell polarity regulation. Nat. Genet. 40, 69–77.

Krahn, M.P., Egger-Adam, D., Wodarz, A., 2009. PP2A Antagonizes Phosphorylation of Bazooka by PAR-1 to Control Apical-Basal Polarity in Dividing Embryonic Neuroblasts. Dev. Cell 16, 901–908.

Landin Malt, A., Dailey, Z., Holbrook-Rasmussen, J., Zheng, Y., Hogan, A., Du, Q., Lu, X., 2019. Par3 is essential for the establishment of planar cell polarity of inner ear hair cells. Proc. Natl. Acad. Sci. 201816333.

Lepelletier, L., de Monvel, J.B., Buisson, J., Desdouets, C., Petit, C., 2013. Auditory Hair Cell Centrioles Undergo Confined Brownian Motion Throughout the Developmental Migration of the Kinocilium. Biophys. J. 105, 48–58.

Liu, Z., Yang, Y., Gu, A., Xu, J., Mao, Y., Lu, H., Hu, W., Lei, Q.-Y., Li, Z., Zhang, M., Cai, Y., Wen, W., 2020. Par complex cluster formation mediated by phase separation. Nat. Commun. 11, 2266.

Mahuzier, A., Gaudé, H.-M., Grampa, V., Anselme, I., Silbermann, F., Leroux-Berger, M., Delacour, D., Ezan, J., Montcouquiol, M., Saunier, S., Schneider-Maunoury, S., Vesque, C., 2012. Dishevelled stabilization by the ciliopathy protein Rpgrip1l is essential for planar cell polarity. J. Cell Biol. 198, 927–940.

Mathewson, A.W., Berman, D.G., Moens, C.B., 2019. Microtubules are required for the maintenance of planar cell polarity in monociliated floorplate cells. Dev. Biol.

Matsumoto, M., Sawada, M., García-González, D., Herranz-Pérez, V., Ogino, T., Bang Nguyen, H., Quynh Thai, T., Narita, K., Kumamoto, N., Ugawa, S., Saito, Y., Takeda, S., Kaneko, N., Khodosevich, K., Monyer, H., García-Verdugo, J.M., Ohno, N., Sawamoto, K. 2019. Dynamic Changes in Ultrastructure of the Primary Cilium in Migrating Neuroblasts in the Postnatal Brain. J Neurosci39(50):9967-9988.

Matsuzawa, K., Akita, H., Watanabe, T., Kakeno, M., Matsui, T., Wang, S., Kaibuchi, K., 2016. PAR3-aPKC regulates Tiam1 by modulating suppressive internal interactions. Mol. Biol. Cell 27, 1511–1523.

May-Simera, H.L., Petralia, R.S., Montcouquio,l M., Wang, Y.X., Szarama, K.B., Liu, Y., Lin, W., Deans, M.R., Pazour, G.J., Kelley, M.W. 2015. Ciliary proteins Bbs8 and Ift20 promote planar cell polarity in the cochlea. Development. 142(3):555-66.

Megason, S.G., 2009. In Toto Imaging of Embryogenesis with Confocal Time-Lapse Microscopy. In: Lieschke, G.J., Oates, A.C., Kawakami, K. (Eds.), Zebrafish. Humana Press, Totowa, NJ, pp. 317–332.

Mirzadeh, Z., Han, Y.-G., Soriano-Navarro, M., Garcia-Verdugo, J.M., Alvarez-Buylla, A., 2010. Cilia Organize Ependymal Planar Polarity. J. Neurosci. 30, 2600–2610.

Mitchell, B., Stubbs, J.L., Huisman, F., Taborek, P., Yu, C., Kintner, C., 2009. The PCP Pathway Instructs the Planar Orientation of Ciliated Cells in the Xenopus Larval Skin. Curr. Biol. 19, 924–929.

Momose, T., Kraus, Y., Houliston, E., 2012. A conserved function for Strabismus in establishing planar cell polarity in the ciliated ectoderm during cnidarian larval development. Development 139, 4374–4382.

Montcouquiol, M., Rachel, R.A., Lanford, P.J., Copeland, N.G., Jenkins, N.A., Kelley, M.W., 2003. Identification of Vangl2 and Scrb1 as planar polarity genes in mammals 423, 5.

Moore, R., Theveneau, E., Pozzi, S., Alexandre, P., Richardson, J., Merks, A., Parsons, M., Kashef, J., Linker, C., Mayor, R., 2013. Par3 controls neural crest migration by promoting microtubule catastrophe during contact inhibition of locomotion. Development 140, 4763–4775.

Munson, C., Huisken, J., Bit-Avragim, N., Kuo, T., Dong, P.D., Ober, E.A., Verkade, H., Abdelilah-Seyfried, S., Stainier, D.Y. 2008. Regulation of neurocoel morphogenesis by Pard6 gamma b. Dev Biol. 324(1):41-54.

Negishi, T., Miyazaki, N., Murata, K., Yasuo, H., Ueno, N., 2016. Physical association between a novel plasma-membrane structure and centrosome orients cell division. eLife 5, e16550.

Nishimura, T., Yamaguchi, T., Kato, K., Yoshizawa, M., Nabeshima, Y., Ohno, S., Hoshino, M., Kaibuchi, K., 2005. PAR-6–PAR-3 mediates Cdc42-induced Rac activation through the Rac GEFs STEF/Tiam1. Nat. Cell Biol. 7, 270–277.

Ohata, S., Herranz-Perez, V., Nakatani, J., Boletta, A., Garcia-Verdugo, J.M., Alvarez-Buylla, A., 2015. Mechanosensory Genes Pkd1 and Pkd2 Contribute to the Planar Polarization of Brain Ventricular Epithelium. J. Neurosci. 35, 11153–11168.

Pouthas, F., Girard, P., Lecaudey, V., Ly, T.B.N., Gilmour, D., Boulin, C., Pepperkok, R., Reynaud, E.G., 2008. In migrating cells, the Golgi complex and the position of the centrosome depend on geometrical constraints of the substratum. J. Cell Sci. 121, 2406–2414.

Rastegar, S., Albert, S., Le Roux, I., Fischer, N., Blader, P., Müller, F., Strähle, U., 2002. A Floor Plate Enhancer of the Zebrafish netrin1 Gene Requires Cyclops (Nodal) Signalling and the Winged Helix Transcription Factor FoxA2. Dev. Biol. 252, 1–14.

Redemann, S., Pecreaux, J., Goehring, N.W., Khairy, K., Stelzer, E.H.K., Hyman, A.A., Howard, J., 2010. Membrane Invaginations Reveal Cortical Sites that Pull on Mitotic Spindles in One-Cell C. elegans Embryos. PLoS ONE 5, e12301.

Ross, A.J., May-Simera, H., Eichers, E.R., Kai, M., Hill, J., Jagger, D.J., Leitch, C.C., Chapple, J.P., Munro, P.M., Fisher, S., Tan, P.L., Phillips, H.M., Leroux, M.R., Henderson, D.J., Murdoch, J.N., Copp, A.J., Eliot, M.-M., Lupski, J.R., Kemp, D.T., Dollfus, H., Tada, M., Katsanis, N., Forge, A., Beales, P.L., 2005. Disruption of Bardet-Biedl syndrome ciliary proteins perturbs planar cell polarity in vertebrates. Nat. Genet. 37, 1135–1140.

Saturno, D.M., Castanzo, D.T., Williams, M., Parikh, D.A., Jaeger, E.C., Lyczak, R., 2017. Sustained centrosome-cortical contact ensures robust polarization of the one-cell C. elegans embryo. Dev. Biol.

Schmoranzer, J., Fawcett, J.P., Segura, M., Tan, S., Vallee, R.B., Pawson, T., Gundersen, G.G., 2009. Par3 and Dynein Associate to Regulate Local Microtubule Dynamics and Centrosome Orientation during Migration. Curr. Biol. 19, 1065–1074.

Schouteden, C., Serwas, D., Palfy, M., Dammermann, A. 2015. The ciliary transition zone functions in cell adhesion but is dispensable for axoneme assembly in C. elegans. J Cell Biol. 210(1):35-44.

Sepich, D.S., Usmani, M., Pawlicki, S., Solnica-Krezel, L., 2011. Wnt/PCP signaling controls intracellular position of MTOCs during gastrulation convergence and extension movements. Development 138, 543–552.

Shimada, Y., Yonemura, S., Ohkura, H., Strutt, D., Uemura, T., 2006. Polarized Transport of Frizzled along the Planar Microtubule Arrays in Drosophila Wing Epithelium. Dev. Cell 10, 209–222.

Siletti, K., Tarchini, B., Hudspeth, A.J., 2017. Daple coordinates organ-wide and cell-intrinsic polarity to pattern inner-ear hair bundles. Proc. Natl. Acad. Sci. 201716522.

Solnica-Krezel, L., Stemple, D.L., Mountcastle-Shah, E., Rangini, Z., Neuhauss, S.C.F., Malicki, J., Schier, A.F., Stainier, D.Y.R., Zwartkruis, F., Abdelilah, S., Driever, W., 1996. Mutations affecting cell fates and cellular rearrangements during gastrulation in zebrafish. Development 123:67-80.

Song, H., Hu, J., Chen, W., Elliott, G., Andre, P., Gao, B., Yang, Y., 2010. Planar cell polarity breaks bilateral symmetry by controlling ciliary positioning. Nature 466, 378–382.

Takagishi, M., Esaki, N., Takahashi, K., Takahashi, M., 2020. Cytoplasmic Dynein Functions in Planar Polarization of Basal Bodies within Ciliated Cells. iScience 23, 101213.

Tarchini, B., Jolicoeur, C., Cayouette, M., 2013. A Molecular Blueprint at the Apical Surface Establishes Planar Asymmetry in Cochlear Hair Cells. Dev. Cell 27, 88–102.

Thouvenin, O., Keiser, L., Cantaut-Belarif, Y., Carbo-Tano, M., Verweij, F., Jurisch-Yaksi, N., Bardet, P.-L., van Niel, G., Gallaire, F., Wyart, C., 2020. Origin and role of the cerebrospinal fluid bidirectional flow in the central canal. eLife 9, e47699.

Tinevez, J.-Y., Perry, N., Schindelin, J., Hoopes, G.M., Reynolds, G.D., Laplantine, E., Bednarek, S.Y., Shorte, S.L., Eliceiri, K.W., 2017. TrackMate: An open and extensible platform for single-particle tracking. Methods 115, 80–90.

Vladar, E.K., Bayly, R.D., Sangoram, A.M., Scott, M.P., Axelrod, J.D., 2012. Microtubules Enable the Planar Cell Polarity of Airway Cilia. Curr. Biol. 22, 2203–2212.

von Trotha, J.W., Campos-Ortega, J.A., Reugels, A.M. 2006 . Apical localization of ASIP/PAR-3:EGFP in zebrafish neuroepithelial cells involves the oligomerization domain CR1, the PDZ domains, and the C-terminal portion of the protein. Dev Dyn. 235(4):967-77.

Wallingford, J.B., 2010. Planar cell polarity signaling, cilia and polarized ciliary beating. Curr. Opin. Cell Biol. 22, 597–604.

Wei, X., Cheng, Y., Luo, Y., Shi, X., Nelson, S., Hyde, D.R., 2004. The zebrafish Pard3 ortholog is required for separation of the eye fields and retinal lamination. Dev. Biol. 269, 286–301.

Wittmann, T., Bokoch, G.M., Waterman-Storer, C.M., 2004. Regulation of Microtubule Destabilizing Activity of Op18/Stathmin Downstream of Rac1. J. Biol. Chem. 279, 6196–6203.

Yi, J., Wu, X., Chung, A.H., Chen, J.K., Kapoor, T.M., Hammer, J.A., 2013. Centrosome repositioning in T cells is biphasic and driven by microtubule end-on capture-shrinkage. J. Cell Biol. 202, 779–792.

Zhang, H., Macara, I.G., 2006. The polarity protein PAR-3 and TIAM1 cooperate in dendritic spine morphogenesis. Nat. Cell Biol. 8, 227–237.

FIGURES

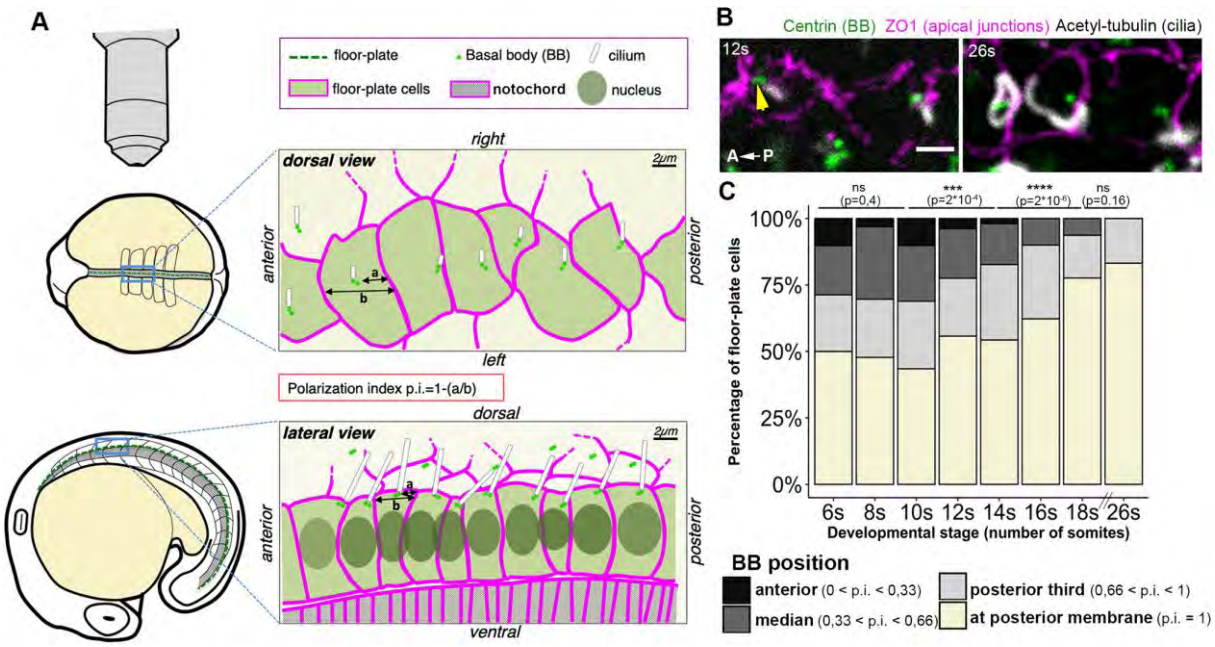

Figure 1 Zebrafish floor-plate progressive planar polarization during somitogenesis.

A) Experimental set-up used to study floor-plate planar polarization in fixed or live embryos. Early (4-12s) or late (after 18s) stage embryos, which displayed floor-plate cells with large apical surfaces were usually imaged from the top (dorsal view, upper part of the figure, see also b)), whereas embryos at intermediate stages (with narrower apical surfaces) were imaged from the side (lateral view, bottom half of the figure). A polarization index (defined as p.i.=1-(a/b) where “a” is the distance between the BB and the posterior membrane and “b” the distance between anterior and posterior membranes) was used to quantify BB position along the antero-posterior axis. **B-C)** Time-course of floor-plate polarization between 6 s and 26 s **B)** Dorsal views of the floor-plate of flat-mounted embryos showing immunostaining against Centrin (green, BB), ZO1 (magenta, apical junctions) and Acetylated-Tubulin (white, cilia) at 12 s (left) and 26 s (right). Cilia are already visible at 12 s but are much

longer at 26 s. The yellow arrow points at an anterior BB bearing a cilium. Scale bar: 2 µm **C)** Quantification of BB position measured from immuno-stained samples as shown in a. BB position along the anterior-posterior axis was quantified using the polarization index. Cells were allocated to different categories depending on their polarization index for each stage (6 s: 7 embryos, 108 cells ; 8 s: 14 embryos, 224 cells ; 10 s: 14 embryos, 354 cells ; 12 s: 5 embryos, 156 cells ; 14 s: 9 embryos, 208 cells ; 16 s: 9 embryos, 220 cells ; 18 s: 5 embryos, 143 cells ; 26 s: 4 embryos, 119 cells). Statistics: Wilcoxon test.

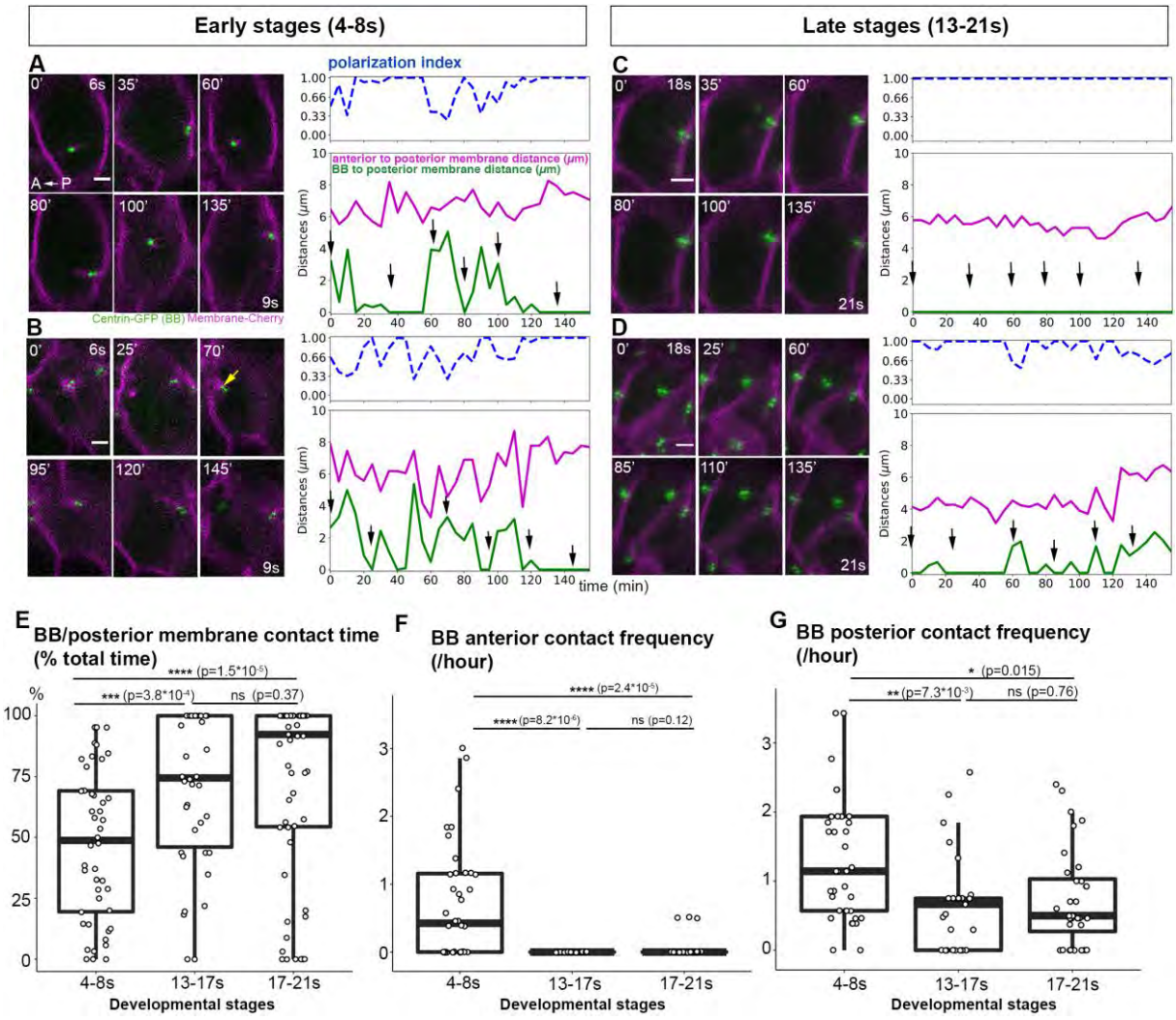

Figure 2 Floor-plate planar polarization involves a change in basal body (BB) motile behaviour.

A-D) Live imaging of BB movements during polarization. Images were taken every 5 minutes; selection of images from two early stage embryos (**A, B,** movies between 6 s and 9 s; yellow arrow in b points at an anterior contact) and two late stage embryos (**C, D,** movies between 18 s and 21 s). The distances between BBs and posterior membranes (green curve) and between the anterior and posterior membranes (magenta curve) and the p.i. (dashed blue curve) were plotted. Black arrows on the graphs indicate the position of the images displayed on the left. **E)** Quantification of

the percentage of total movie time spent by the BB in contact with the posterior membrane (i.e. centrin-GFP and mb-Cherry abut or overlap at the posterior cell membrane). (4-8s: 5 embryos, 41 cells; 13-17s: 6 embryos, 38 cells; 17-21s: 7 embryos, 59 cells). **F, G)** Number of contacts per hour between BB and anterior (**F**) or posterior (**G**) membrane at different stages: 4 to 8 s (5 embryos, 41 cells), 13 to 17 s (5 embryos, 25 cells) and 17 to 21 s (7 embryos, 32 cells). Cells with a BB in contact with the posterior membrane during the whole movie (points at 100% in Fig. 1E) were not plotted in F and G. Statistics: Wilcoxon test. Scale bars: 2 μm.

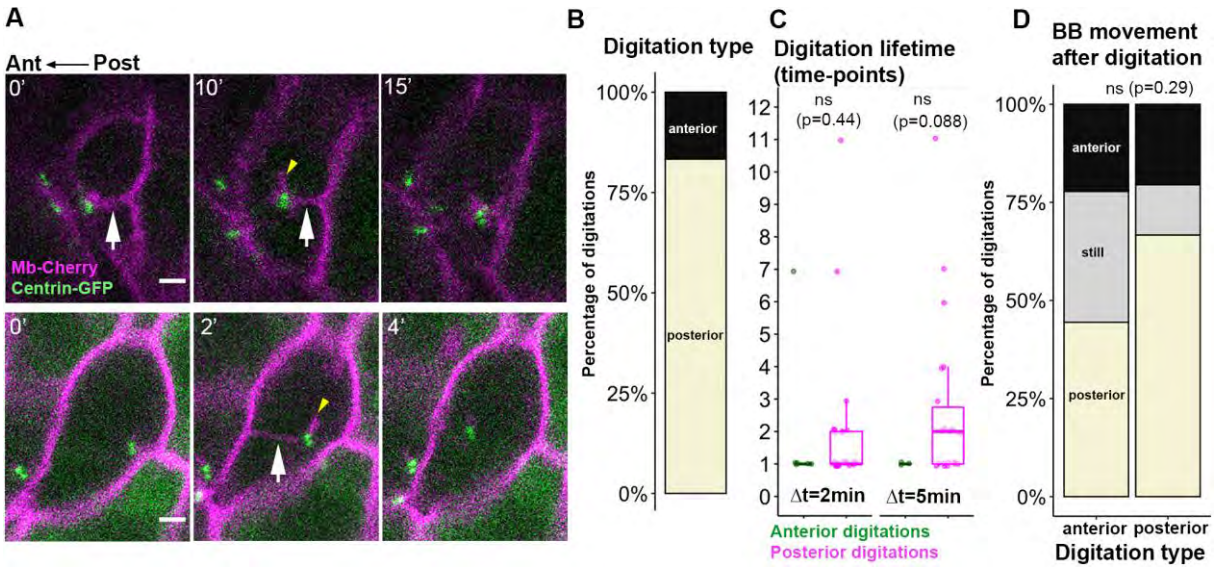

Figure 3 Membrane digitations link BBs to ant/post membranes during FP polarization

A) Images from live-imaging (Δt = 2 or 5 min) showing a posterior (top) and an anterior (bottom) digitation (white arrows). Time (in min) is indicated in the upper-left corner. Short mbCherry-positive digitations, presumably cilia, were in some cases associated to the BB (yellow arrowheads). **B)** Proportion of posterior and anterior digitations (54 digitations, 8 embryos, 22 cells) **C)** Number of timepoints where anterior or posterior digitations were detected in movies with Δt = 2 or 5 minutes (Δt2min: 6 anterior, 23 posterior digitations, 4 embryos, 8 cells. Δt5min: 3 anterior and 22 posterior digitations, 3 embryos, 13 cells, Wilcoxon tests). Digitations were most often observed on a single or two consecutive timeframes. **D)** BB movements after anterior (left bar) or posterior digitation (48 digitations, 8 embryos, 22 cells, Fisher test).

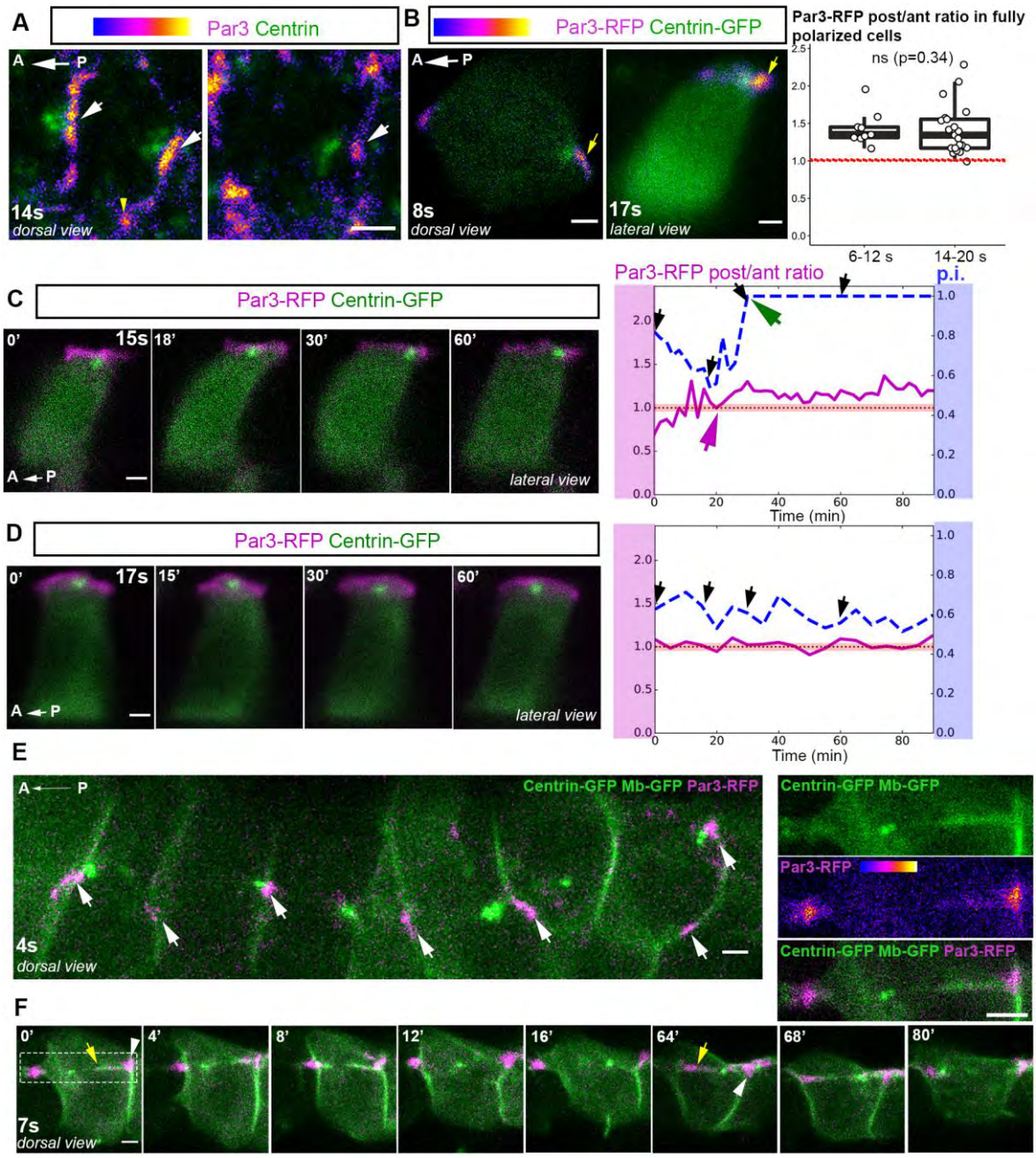

Figure 4. Par3 is asymmetrically localized in FP cells and forms patches at which almost all BB/membrane contacts occur.

A) Individual FP cells from dorsal views of 14 s embryos showing Par3 immunofluorescence. Par3 localizes at apical junctions and is enriched at tricellular junctions (yellow arrowhead) and in patches at ant/post membranes (white arrows), whether the BB is in contact with the posterior membrane (left image) or not (right image). **B)** Representative images of mosaically labelled FP cells expressing Par3-

RFP and Centrin-GFP at early (8 s, left) or late (17 s, right) stages. Yellow arrows point at posterior Par3-RFP enrichment. Boxplots on the right show quantification of Par3-RFP posterior/anterior fluorescence intensity ratio in fully polarized FP cells at early and late stages. The red dotted line indicates a ratio of 1 (6-12s, mean ratio= 1.42, 7 embryos, 9 cells; 14-20s mean ratio =1.38, 13 embryos, 21 cells, Wilcoxon test). **C-D)** Images of time-lapse movies showing individual FP cells from embryos mosaically expressing Par3-RFP (magenta) and centrin-GFP (green) (lateral view). Par3-RFP posterior/anterior fluorescence intensity ratio is plotted on the right plots (magenta curve) along with the polarization index (« p.i. », dashed blue curve). Black arrows indicate time-points shown on the left. **C)** FP cell with Par3 posterior enrichment in an embryo filmed between 15 s and 17 s. Par3 posterior enrichment starts 20 min after the beginning of the movie (magenta arrow), 10 min before BB/posterior membrane contact (green arrow). **D)** FP cell with no posterior Par3 enrichment (Par3-RFP post/ant ratio close to 1) with a BB oscillating around the middle of the apical surface, in an embryo filmed between 17 s and 19 s. **E-F)** Images from movies of early stage embryos mosaically injected with centrin-GFP (green), Membrane-GFP (green) and Par3-RFP (magenta) mRNAs. All pictures are dorsal views of FP cells. **E)** Global view of 6 adjacent FP cells; white arrows point at Par3 patches (aligned along the AP axis) with which BBs will make contacts during the movie. **F)** Example of a BB moving back and forth and contacting the membrane at Par3 patches. Posterior and anterior membrane digitations originating from Par3 patches and partially coated with Par3 can also be seen. Yellow arrows point to posterior (t=0') and anterior (t=64') digitations. White arrowheads point to Par3 patches. Par3 patch deformation can be seen at t=64' and at t=0' (images on the right show a close-up on the framed region at t=0'). Scale bars: 2µm.

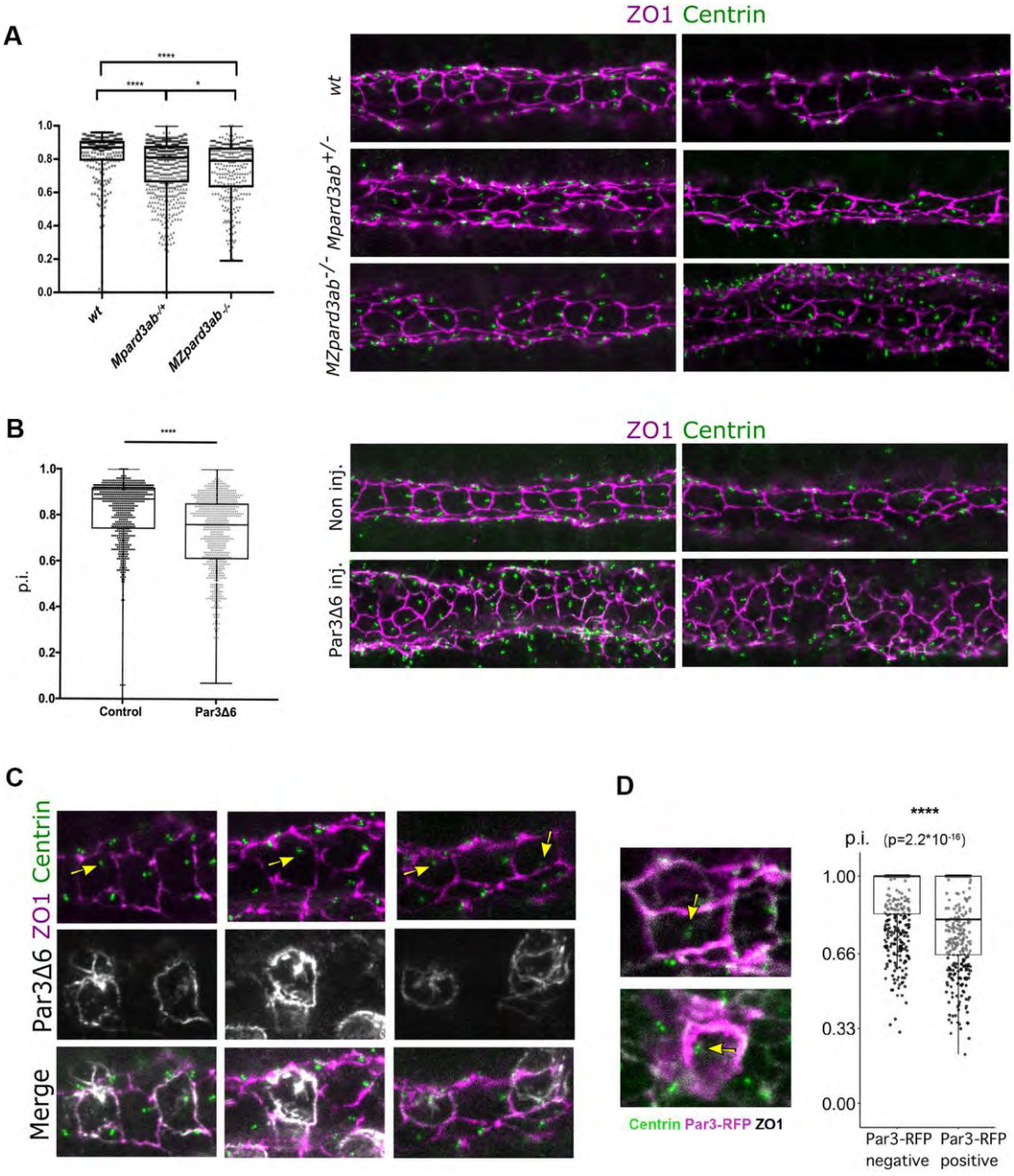

Figure 5. Disruption of FP polarization by Par3 depletion or perturbed localization

A) Polarization index (p.i.) of FP cells from wt (638 cells from 9 embryos), *MPard3ab*$^{+/-}$ (644 cells from 13 embryos) and *MZPard3ab*$^{-/-}$ (303 cells from 6 embryos) 22s embryos. **B)** Polarization index (p.i.) of FP cells from control (596 cells from 11 embryos) or Par3Δ6-GFP-overexpressing (750 cells from 8 embryos)

embryos. Each dot represents one cell. Representative immunofluorescence images are shown on the right. **C)** Representative images of FP cells from embryos mosaically expressing Par3Δ6-GFP. Yellow arrows point to BB position coinciding with high GFP expression in Par3Δ6-GFP overexpressing cells. **D)** Polarization index (p.i.) of Par3-RFP negative and positive FP cells from embryos mosaically over-expressing Par3-RFP. Left: representative immunostaining pictures; yellow arrows point at mispositioned BBs in Par3-RFP over-expressing cells (538 Par3-RFP negative cells and 375 Par3-RFP positive cells from 20 embryos). Scale bar: 5 μm in a-c, 2μm in d. Statistics: Mann-Whitney U (Wilcoxon) test.

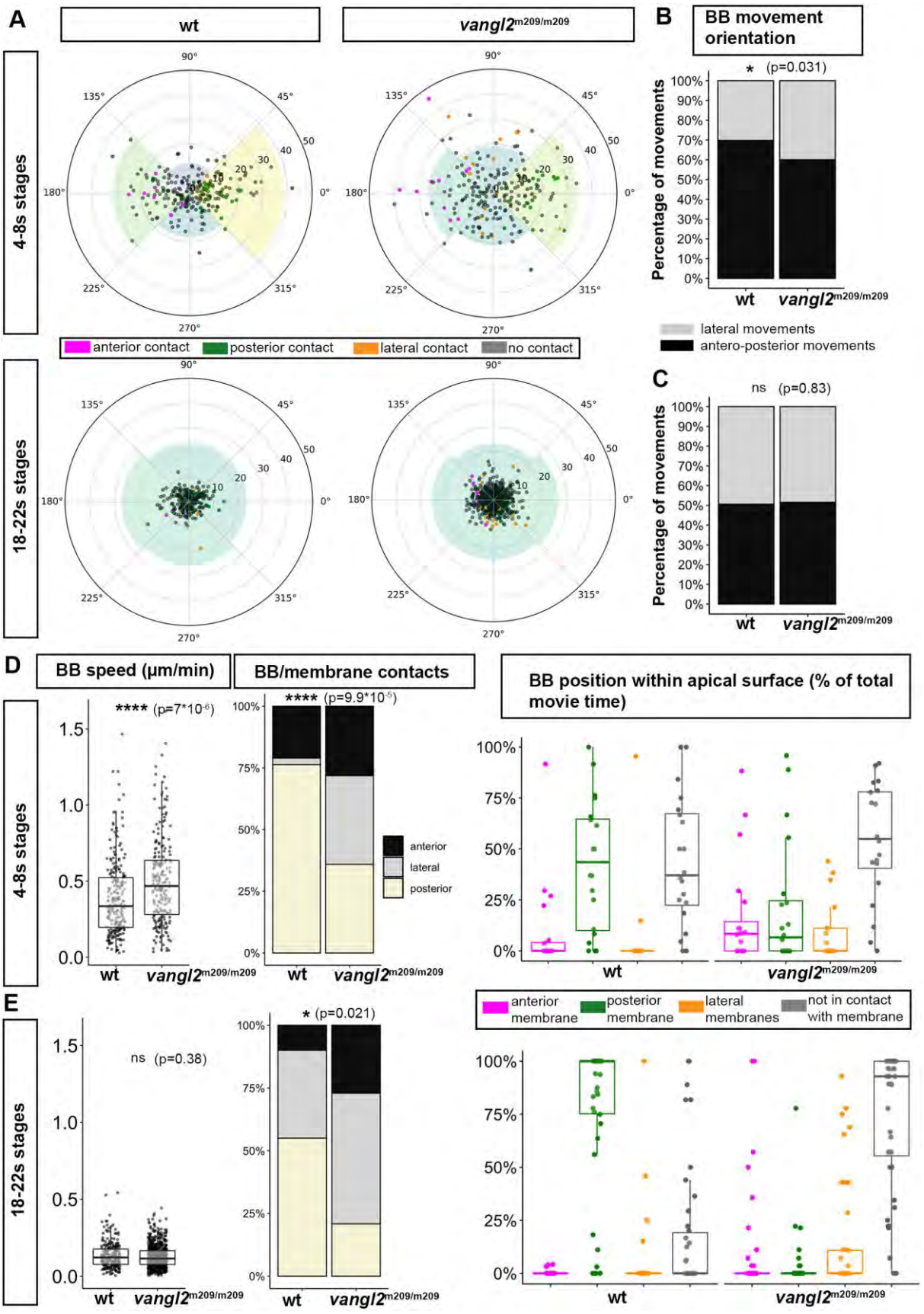

Figure 6 Abnormal BB behaviours in *vangl2*^{m209} mutant FP

A) BB movements in wt (left column) and *vangl2*^{m209} (right column) embryos at early (first line) and late (second line) developmental stages. Each dot represents the endpoint of a single BB movement, the starting point being the center of the circle; thus, the angles outside the circle represent BB movement orientation relative to the embryo antero-posterior axis, and the distance relative to the center of the circle represents its length (circle radius is 7 µm). The color of the dots indicates whether a movement leads to a membrane contact and, if so, the nature of the contact (anterior, posterior or lateral) (early stages: wt 8 embryos, 20 cells, 238 movements; *vangl2*^{m209}: 9 embryos, 20 cells, 220 movements; late stages: wt 4 embryos, 19 cells, 255 movements; *vangl2*^{m209}: 4 embryos, 42 cells, 708 movements). **B, C)** Orientation of BB movements in wt and *vangl2*^{m209} embryos at early (b) or late (c) stages. **D, E)** BB movements speed, nature of membrane contacts and total time spent in contact with membranes at early (D) and late (E) stages. Statistics: Wilcoxon test for BB speed; Fisher test for BB movement orientation and BB/membrane contacts.

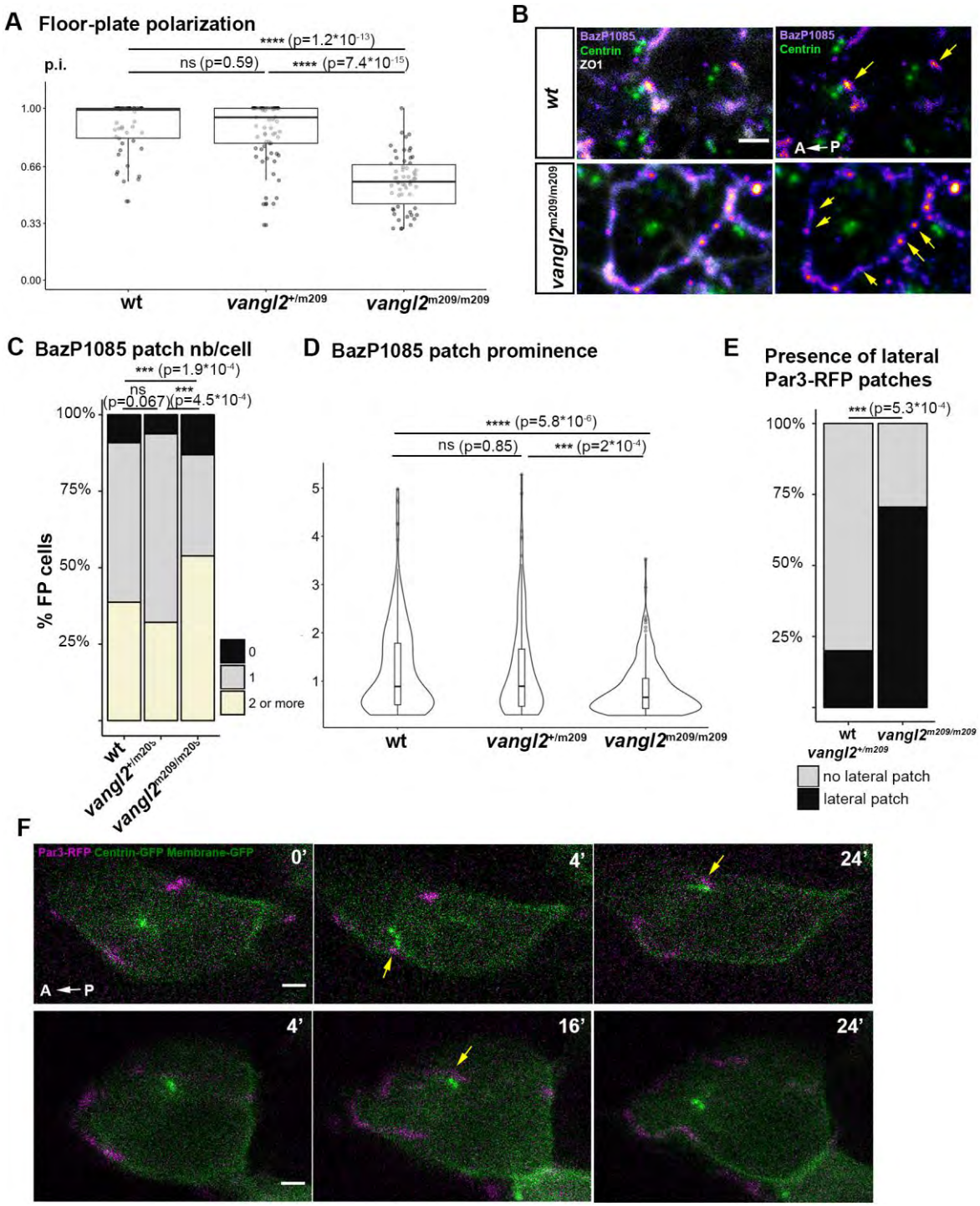

Figure 7 Par3 clustering and localization in *vangl2*^{m209} FP

A) Polarization index of *vangl2*$^{m209/m209}$ determined from immunostaining data. wt: 2 embryos, 49 cells; *vangl2*$^{m209/+}$: 3 embryos, 66 cells; *vangl2*$^{m209/m209}$: 5 embryos, 57 cells. **B)** Immunostaining of phosphorylated Par3 (BazP1085 antibody) in *vangl2*$^{+/+}$

(wt) and *vangl2*$^{m209/m209}$ embryo FP at 18 s. ZO1 staining was removed in the right images to reveal Par3 patches (yellow arrows). **C)** Quantification of Par3 patch number per cell on ant/post membranes from immunostaining data as shown in B. **D)** Prominence of Par3 patches (BazP1085 antibody) in wt and *vangl2*$^{m209/m209}$ mutant embryo FP at 18 s In a-d, *vangl2*$^{+/+}$: 7 embryos, 186 cells ; *vangl2*$^{m209/+}$: 5 embryos, 112 cells ; *vangl2*$^{m209/m209}$: 7 embryos, 129 cells. **E)** Percentage of cells displaying a lateral Par3-RFP patch in live-imaging (such as in F). *vangl2*$^{+/+}$ and *vangl2*$^{m209/+}$: 16 embryos, 45 cells ; *vangl2*$^{m209/m209}$: 7 embryos, 17 cells. **F)** Images from 2 movies of 5s *vangl2*$^{m209/m209}$ embryos mosaically injected with Par3-RFP, Centrin-GFP and Membrane-GFP mRNA at the 16-32 cell stage. Yellow arrows point at contact events between lateral Par3 patches and BBs. Statistics: Wilcoxon test for p.i. and prominence; Fisher test for patch number and percentage of cells with lateral patches.

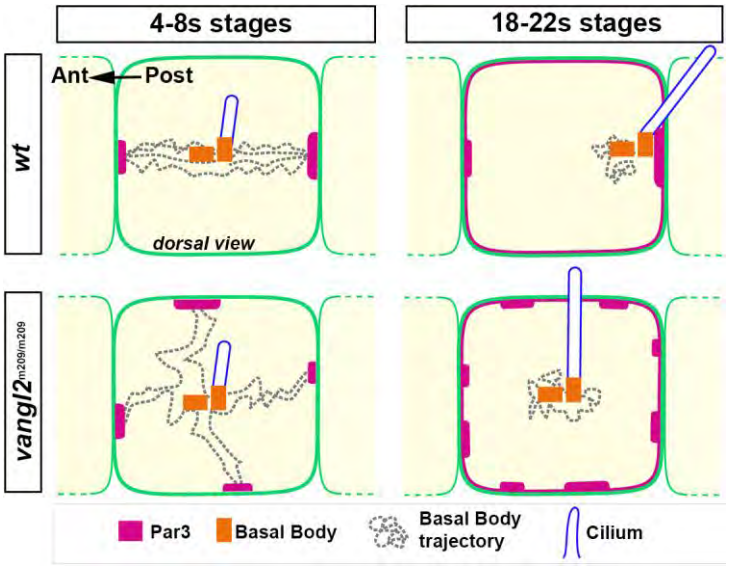

Figure 8 Summary of BB behaviour and Par3 localization at early and late stages in the FP of wt and *vangl2* mutants.

Table S1. Antibodies and plasmids

Antibodies

Antibody	Source	Identifier	Dilution
Mouse monoclonal IgG2a anti-centrin (clone 20H5)	Merck Millipore	# 04-1624 RRID: AB_10563501	1:200
Mouse monoclonal IgG1 anti-ZO1 (clone ZO1-1A12)	Invitrogen	RRID: AB_2533147	1:400
Mouse monoclonal IgG2b anti-acetylated-tubulin (clone 6-11B-1)	Sigma-Aldrich	#T 6793 RRID: AB_477585	1:400
Rabbit polyclonal anti-Par3	Merck Millipore	#07-330 RRID:AB_11213581	1:200
Rabbit polyclonal anti-phosphorylated-Ser1085-Bazooka	(Krahn et al., 2009)	N/A	1:200
Rabbit polyclonal anti-DsRed	Takara	# 632496 RRID:AB_10013483	1:400
Mouse IgG1 anti-FLAG (M2)	Sigma	F3165	1:100
Goat anti-mouse IgG1 Alexa633	Molecular probes	# A-21126 RRID:AB_2535768	1:400

Goat anti-mouse IgG2a Alexa568	Molecular probes	# A-21134 RRID:AB_2535773	1:400
Goat anti-mouse IgG2a Alexa488	Molecular probes	# A-21131 RRID:AB_141618	1:400
Goat anti-mouse IgG2b Alexa633	Molecular probes	# A-21146 RRID:AB_2535782	1:400
Goat anti-rabbit IgG Alexa568	Molecular probes	# A-11011 RRID:AB_143157	1:400

Plasmids

Constructs	Source
pCS2-Membrane-Cherry	Megason, 2009
pCS2-GFPhumcentrin1	Pouthas et al., 2008
pCS2+-Par3-RFP	Alexandre et al., 2010
pCS2+-Par3Δ6-GFP	von Trotha et al., 2006

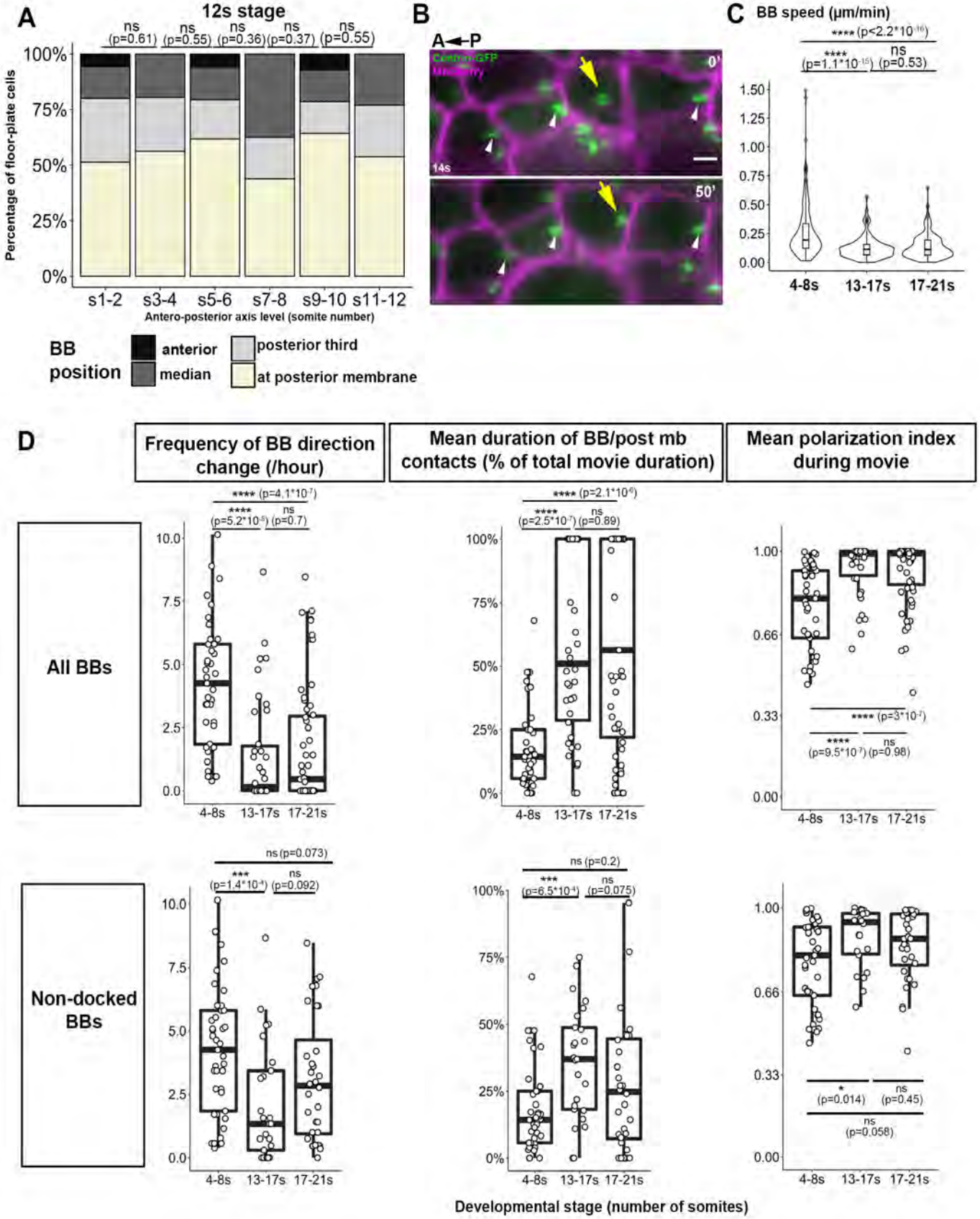

Figure S1 Donati et al.

Figure S1. Further characterization of FP polarization in space and time.

A) Quantification of FP polarization along the AP axis at 12 s. Analysis was performed on fixed immunostained embryos as described in Fig. 1A. Comparison between stages was done using a Wilcoxon test. **B)** Still images from FP BB (green) and membrane (magenta) live imaging (dorsal view, start at 14s stage). The yellow arrow points to BB that will move and make contacts with the posterior membrane between 0 and 50 min after the movie started. White arrowheads point at BBs in adjacent cells that stay in contact with the posterior membrane during this time interval. **C)** BB speed measured from live-imaging data at different developmental stages. The speed of each BB movement was calculated by dividing the value of BB/posterior membrane variations (corresponding to green curves in Fig. 1c-f) by the total duration of the movement (4-8s: 4 embryos, 38 cells; 13-17s: 6 embryos, 22 cells; 17-21s: 7 embryos, 32 cells). Comparison between stages was done using a Wilcoxon test. **D)** Movies described in Fig. 1 were used to quantify BB direction change frequency, mean duration of BB/posterior membrane contact events as a percentage of total imaging duration and mean polarization index during live-imaging. Plots in the first line take-into-account the BBs that stay in contact with the posterior membrane 100% of movie duration (posteriorly docked BBs) whereas the second line only represents BBs that are not posteriorly docked. Comparison between stages was done using a Wilcoxon test. Scale bar: 2µm.

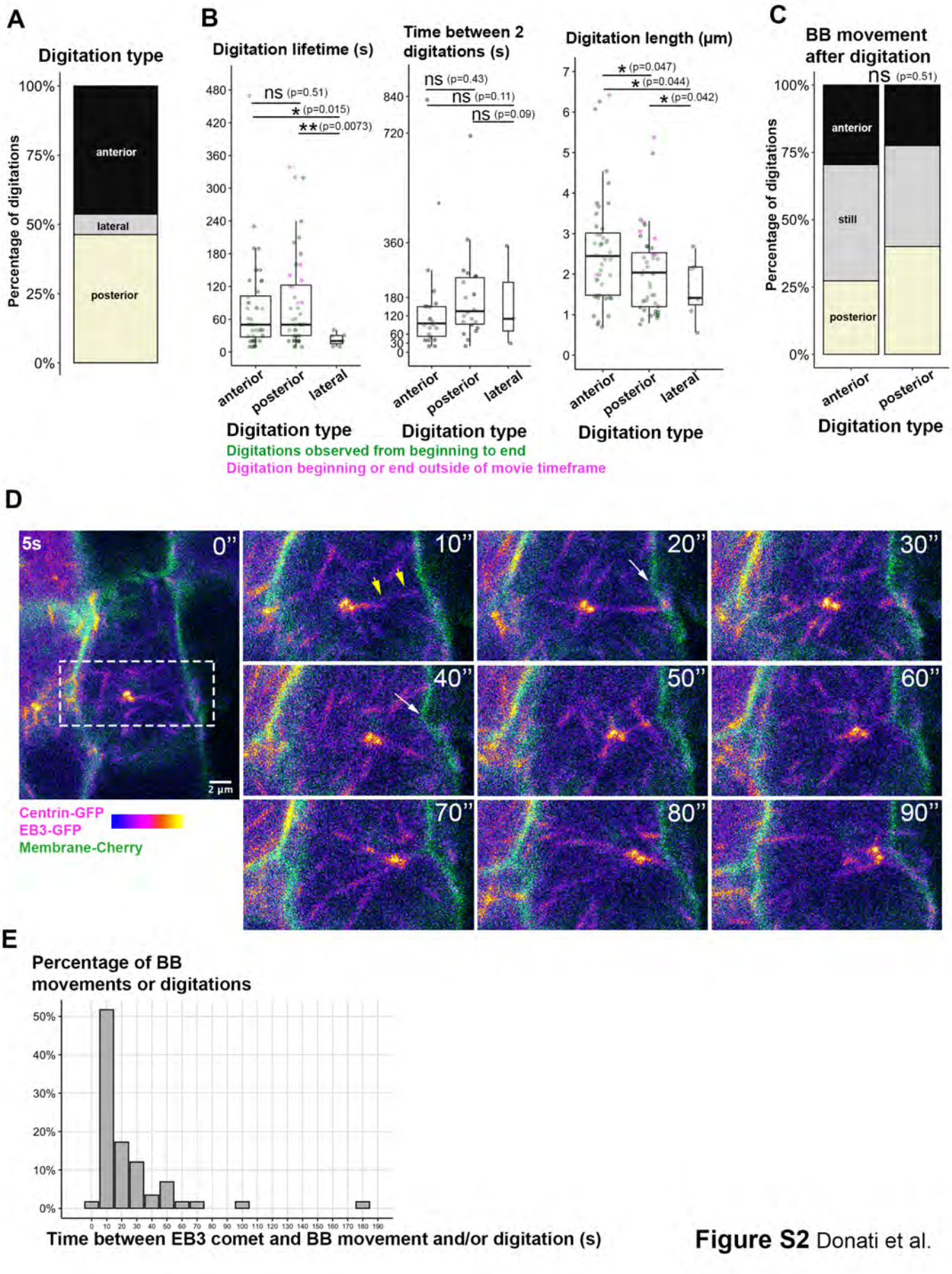

Figure S2 Donati et al.

Figure S2. High temporal resolution imaging reveals numerous anterior and posterior digitations and dynamic microtubules between BB and target membrane

A-C) Characterization of digitations with high temporal resolution live-imaging (one image every 10sec) (12 embryos, 20 cells, 44 anterior digitations, 44 posterior digitations, 7 lateral digitations). **A)** Repartition of digitation types. Anterior, lateral and posterior correspond to the membrane from which the digitation forms. There were as many anterior as posterior digitations, in contrast to what we observe in our Δt=2 or 5 min movies (Fig. 3) **B)** Quantification of digitation lifetime, recurrence time (time elapsed before a particular digitation reforms at the same spot) and maximal length. Digitations had a median lifetime of 50 sec and a median length of 2 µm. Most digitations formed at a spot where we could previously see another digitation ("recurrent" digitations, 85%, 44/52) with a median time-lapse of 70sec. Dots in magenta correspond to digitations that had formed before the beginning of live-imaging or had not disappeared yet when we stopped filming, and for which we could not determine the exact lifetime (which is thus under-estimated) (comparison done with Wilcoxon test). **C)** Direction of BB movements after an anterior (left) or posterior (right) digitation disappears. The BB either moved anteriorly, posteriorly or remained still: (comparison done with Fisher test). There was no difference in digitation lifetime, which median value was 50sec both for anterior and posterior digitations. The time elapsed between two recurrent digitations was also not significantly different between anterior (median of 70sec) and posterior (median of 80sec) digitations. The presence of more posterior digitations in Δt2min and Δt5min movies but not in Δt10sec movies could be due to the fact that we miss most very short-lived digitations in Δt2min or Δt5min movies

and that the short duration of our Δt10sec movies (in average 20min long) prevented us to see some long-lived digitations from extension to retraction (pink dots). Anterior and posterior digitations had similar size of around 2µm, although anterior digitations were slightly longer (2.4µm), probably due to the fact that BBs even at these early stages have a posteriorly biased position (Fig. S1D Mean polarization index plots). Posterior digitations were followed by a posteriorward BB movement in 40% of cases (16/40) whereas anterior digitations were followed by an anteriorward BB movement in only 30% of cases (13/34) suggesting that digitation formation is probably not a cause but rather a consequence of BB movements. **D)** Dorsal view of a FP cell of a 5s stage embryo mosaically injected with Centrin-GFP (BB), EB3-GFP (microtubule plus ends) and Membrane-Cherry**,** which was then imaged every 10s. The dotted frame corresponds to the enlarged region on the right. Yellow arrows (10"): microtubule extending from the BB toward the spot of the posterior membrane that the BB will reach at t=90". White arrows: membrane digitation forming from the spot targeted by the microtubule highlighted at t=10" and toward the BB. **E)** Time elapsed between an EB3 comet reaching a membrane (such as in a at t=10") and the moment when a digitation forms or the BB starts moving towards this membrane (6 embryos, 10 cells, 58 EB3 comets).

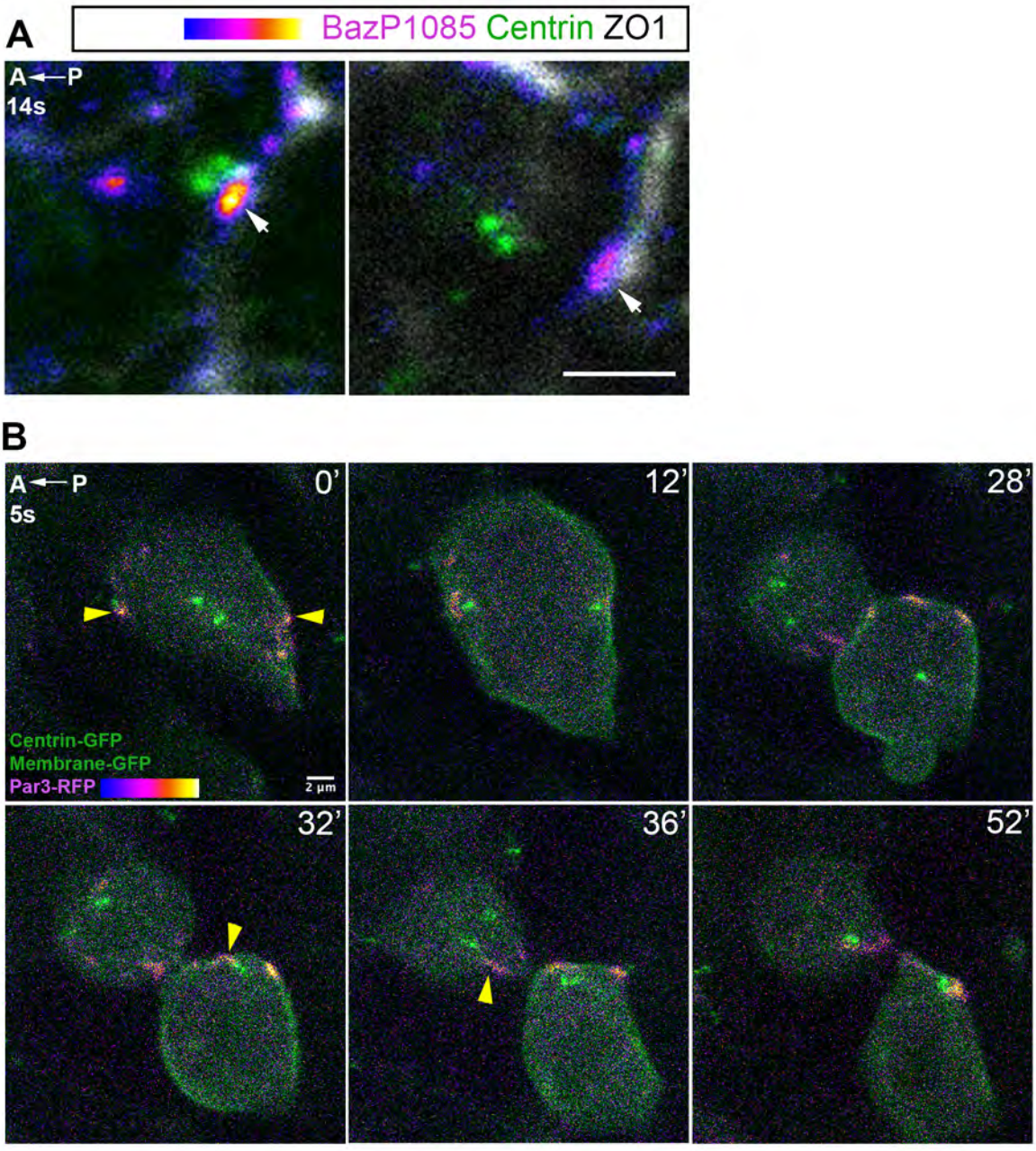

Figure S3 Donati et al.

Figure S3. Par3 phosphorylation in FP cells and rapid migration of centrosome to Par3 patches after mitosis A) Individual cells from dorsal views of 14 s stage embryos showing immunofluorescence with an antibody against Drosophila Par3 (Bazooka/Baz) phosphorylated on Ser1085 (BazP1085) in FP cells. Two distinct cells are shown. phospho-Par3 displays the same patchy localization as total Par3 (Fig4a) White arrows point at patches at ant/post membranes, which are present whether the BB is in contact with the posterior membrane (left images) or not (right image). **B)** Example of FP cell mitosis in an early stage (5s) embryo mosaically injected with Par3-RFP, Centrin-GFP and Membrane-GFP mRNAs and imaged every 4 minutes (Movie S12). Yellow arrows point at Par3-RFP patches, at the onset of mitosis (t=0') and after cytokinesis, when the centrosome makes contact with the Par3 patch, in the posterior daughter cell (t=32') and anterior daughter cell (t=36').

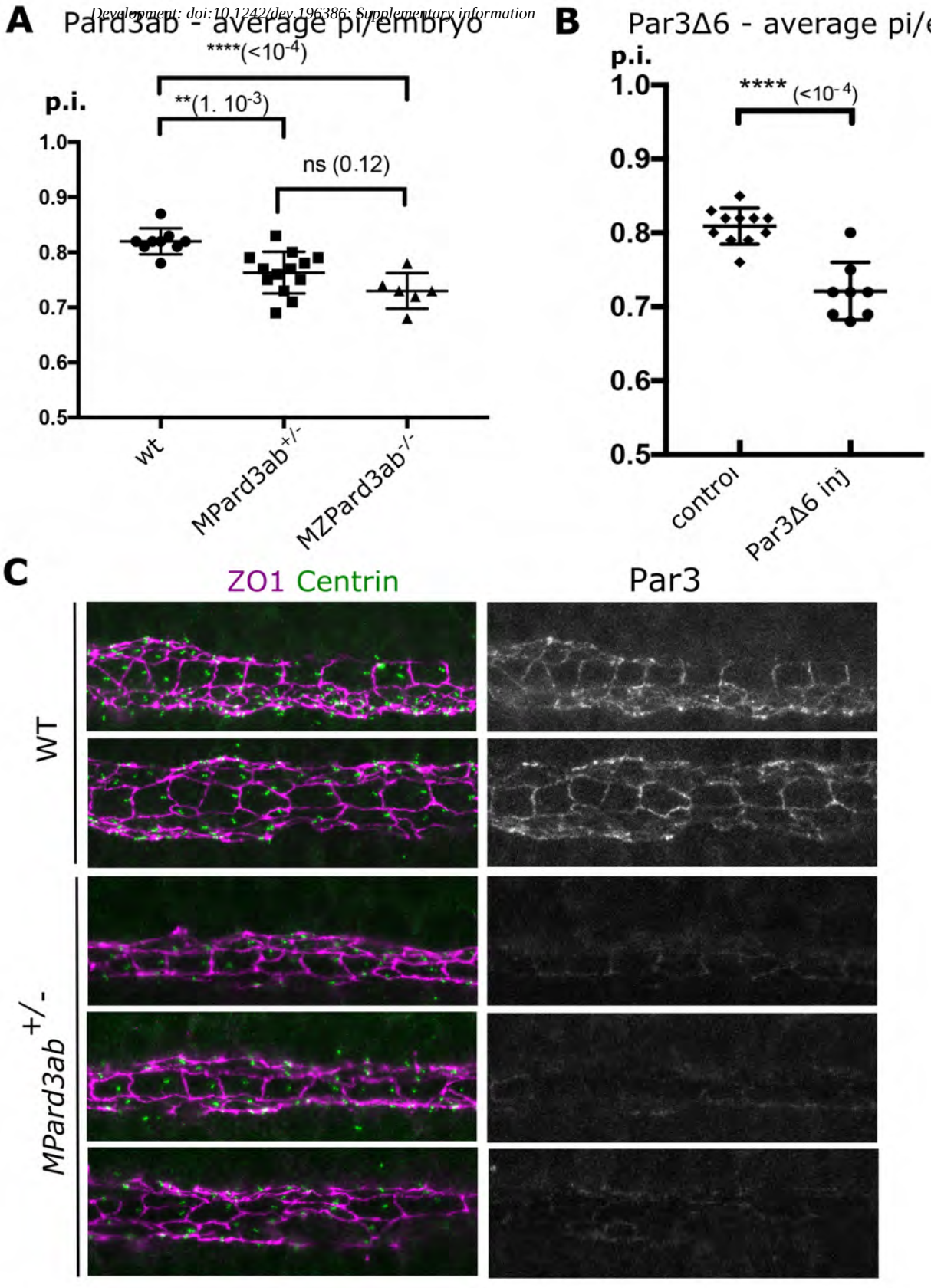

Fig. S4 Donati et al.

Figure S4. Additional Par3 and Vangl2 functional data. **A, B)** Graphs showing the mean p.i. of FP cells analyzed in individual embryos (each dot represents one embryo), in *MZpard3ab* mutants (A) and in Par3Δ6-GFP injection experiments (B). In (A), wt: 9 embryos (> 53 cells/embryo); *Mpard3ab*$^{+/-}$: 13 embryos (> 12 cells/embryo); *MZpard3ab*$^{-/-}$: 6 embryos (> 37 cells/embryo). Anova test shows that the average p.i. is significantly different between *MZpard3ab*$^{-/-}$ and wt embryos (P<10-4). Post-hoc Tukey's multiple comparisons are shown on the graph with P values corrected for multiples tests. In (B), non-injected controls: 11 embryos (> 16 cells/embryo); Par3Δ6-GFP-injected: 8 embryos (> 78 cells/embryo). Unpaired t test with Welch's correction shows that the mean p.i. value is significantly different between controls and Par3Δ6-GFP-injected embryos (P<10-4). **C)** Representative examples of wt and *Mpard3ab*$^{+/-}$ embryos immunostained with ZOI and Centrin (left) or with Par3 (right) antibodies. Par3 immunostaining intensity is strongly reduced in the FP of *Mpard3ab*$^{+/-}$ embryos, in which BB polarization is perturbed. Scale bar 5 μm. **D)** Par3 patch prominence is defined as the height of Par3 fluorescence peak relative to the highest and nearest local fluorescence minimum. For each cell, prominence is normalized by the lowest Par3 intensity value. Yellow arrows: tricellular junctions; white bar: orientation of the fluorescence measurement along the transverse membrane, star: Par3 patch.

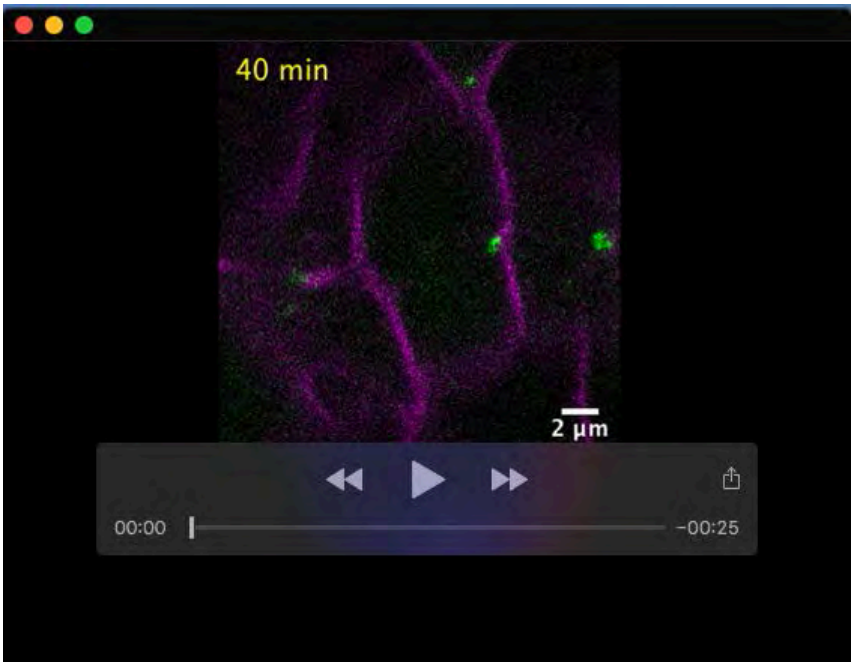

Movie 1. Live imaging of a BB bouncing off the posterior membrane in an earlystage FP cell. wt embryos were injected with Centrin-GFP (green) and membrane-Cherry (magenta) mRNAs at the one-cell stage. White arrows indicate the position of the BB at the first and last time-points. Images were taken every 5 minutes during the 6 s to 9 s stages time-frame. Dorsal view. Corresponds to Fig2A.

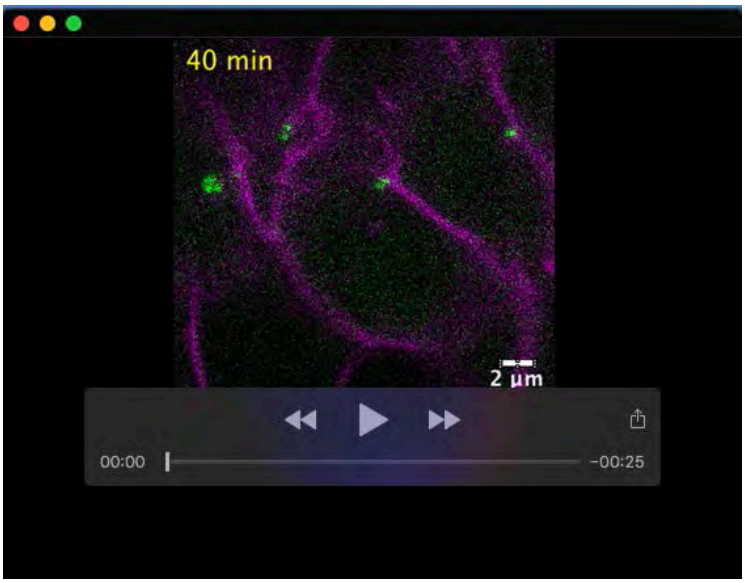

Movie 2. Live imaging of a BB bouncing off posterior and anterior membranes in an early-stage FP cell. wt embryos were injected with Centrin-GFP (green) and membrane-Cherry (magenta) mRNAs at the one-cell stage. White arrows indicate the position of the BB at the first and last time-points. Images were taken every 5 minutes during the 6 s to 9 s stages time-frame. Dorsal view. Corresponds to Fig2B.

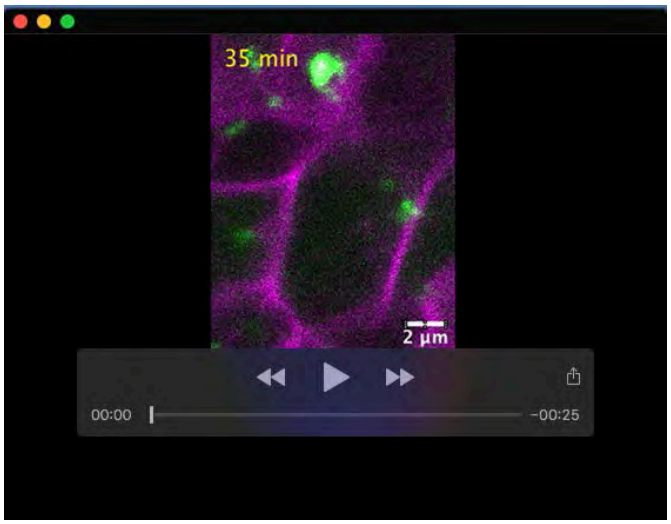

Movie 3. Live imaging of a BB staying in contact with the posterior membrane in a late-stage FP cell. wt embryos were injected with Centrin-GFP (green) and membrane-Cherry (magenta) mRNAs at the one-cell stage. White arrows indicate the position of the BB at the first and last time-points. Images were taken every 5 minutes during the 18 s to 21 s stages time-frame. Dorsal view. Corresponds to Fig2C.

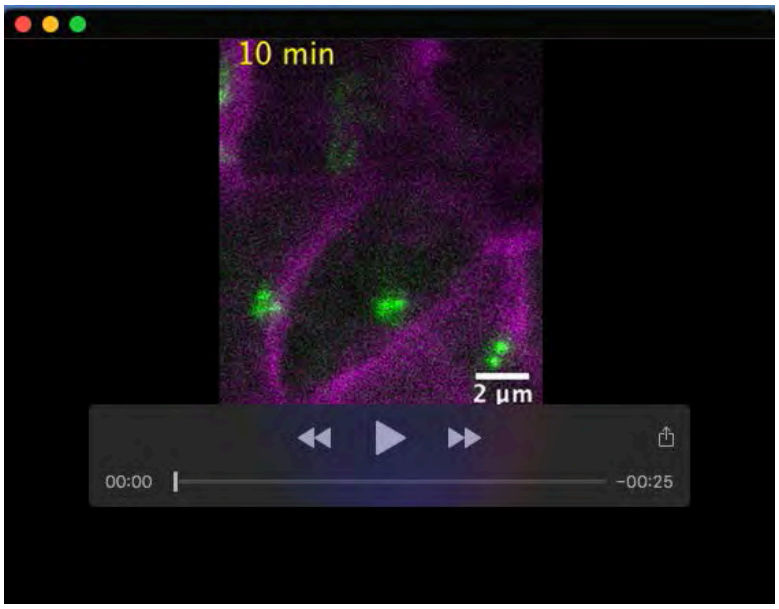

Movie 4. Live imaging of BB bouncing against the posterior membrane in a latestage FP cell. wt embryos were injected with Centrin-GFP (green) and membrane-Cherry (magenta) mRNAs at the one-cell stage White arrows indicate the position of the BB at the first and last time-points. Images were taken every 5 minutes during the 18 s to 21 s stages time-frame. Dorsal view. Corresponds to Fig2D.

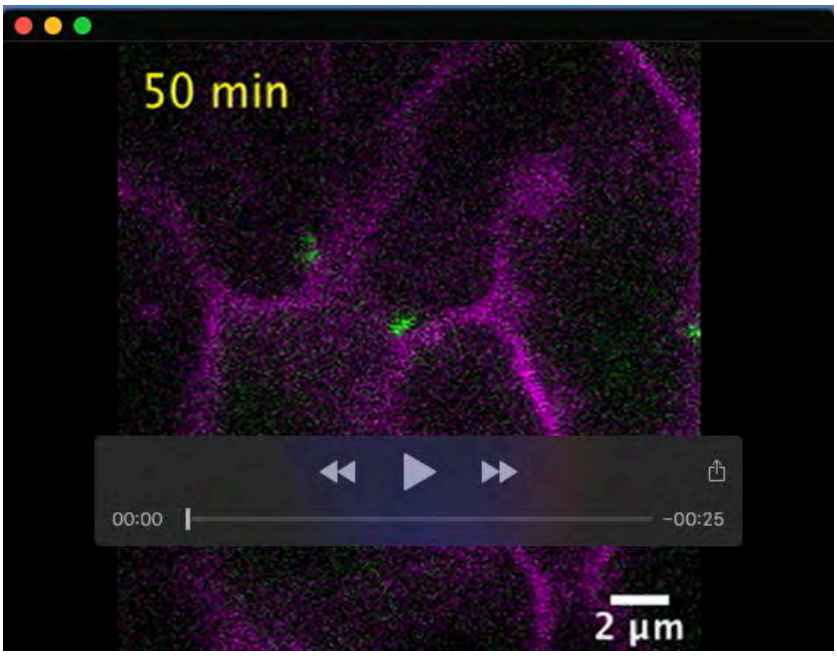

Movie 5. Live imaging of BB movements in a FP cell displaying a membrane digitation between BB and the posterior membrane (yellow arrow at t=115 min). wt embryos were injected with Centrin-GFP (green) and membrane-Cherry (magenta) mRNAs at the one-cell stage. White arrows point at the BB. Images were taken every 5 minutes during the 6 s to 9 s stages time-frame. Dorsal view. Corresponds to Fig3A upper row.

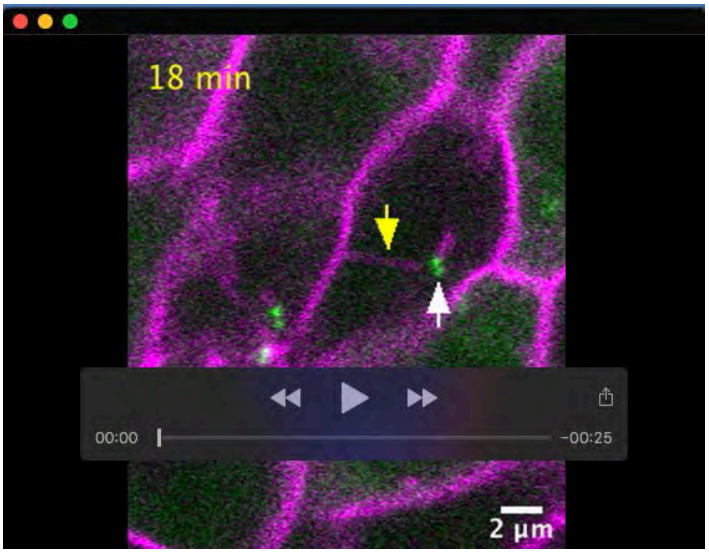

Movie 6. Live imaging of BB movements in a FP cell displaying a membrane digitation between BB and the anterior membrane (yellow arrow at t=18 min). wt embryos were injected with Centrin-GFP (green) and membrane-Cherry (magenta) mRNAs at the one-cell stage. Membrane digitations between the posterior membrane and BB can also be seen at t=10min, t=26min and t=66min. White arrows point at the BB. Images were taken every 2 minutes during the 8 s to 10 s stages time-frame. Dorsal view. Corresponds to Fig3A lower row.

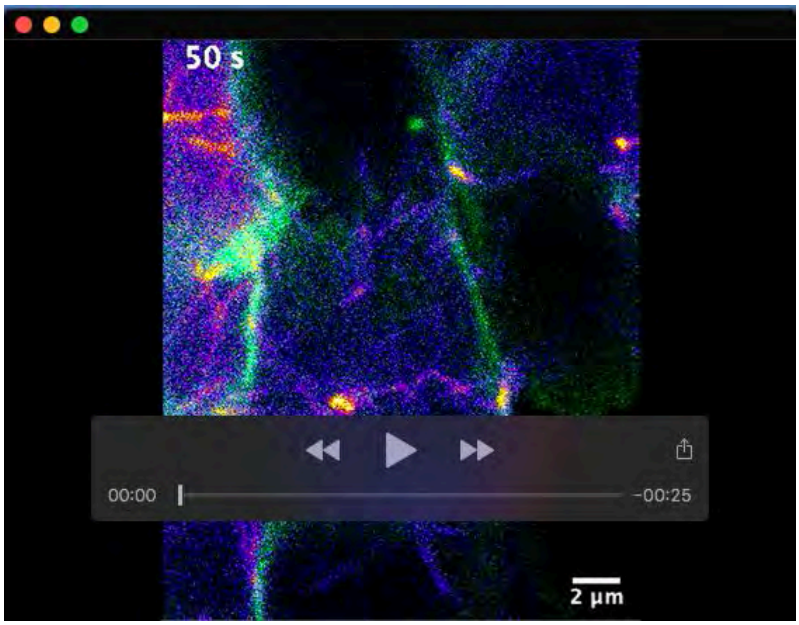

Movie 7. Live imaging of microtubule dynamics and BB movements in a FP cell at the 5s stage. wt embryos were injected with EB3-GFP, Centrin-GFP (Fire LUT, coding for fluorescence intensity) and membrane-Cherry (green) mRNAs at the 16-cell stage. and then imaged for 8min every 10 seconds at the 5s stage. White arrow at t=0" points at the BB. White arrows at t=150", t=160", t=280" and t=290" point at posterior membrane deformation and yellow arrowheads at t=150" and t=280" point at microtubules linking BB and posterior membrane at the spot where the membrane bends and toward which BB will move. Dorsal view. Corresponds to FigS2D.

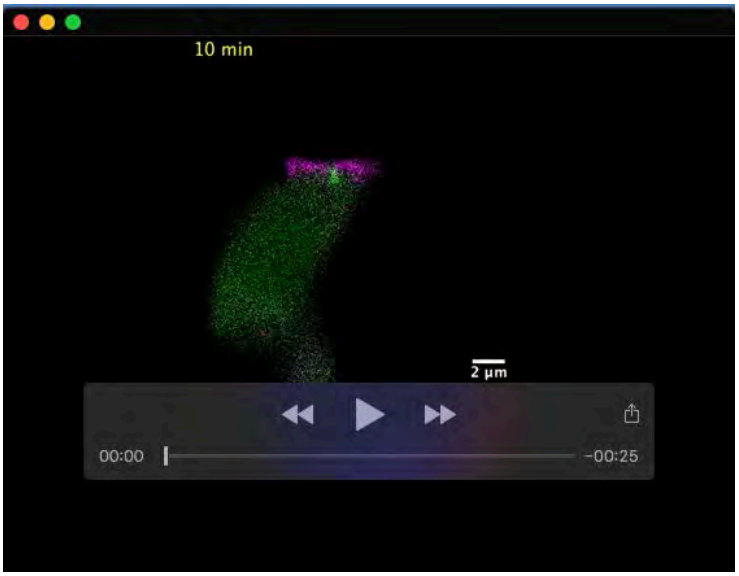

Movie 8. Live imaging of BB movements and Par3-RFP localization in a polarizing FP cell. wt embryos mosaically expressing Centrin-GFP (green) and Par3-RFP (magenta). White arrows point at the BB at t=0 and at t=30 min, when the BB touches the posterior membrane. Images were taken every 2 min during the 15 s to 17 s stages time-frame. Lateral view. Corresponds to Fig4C.

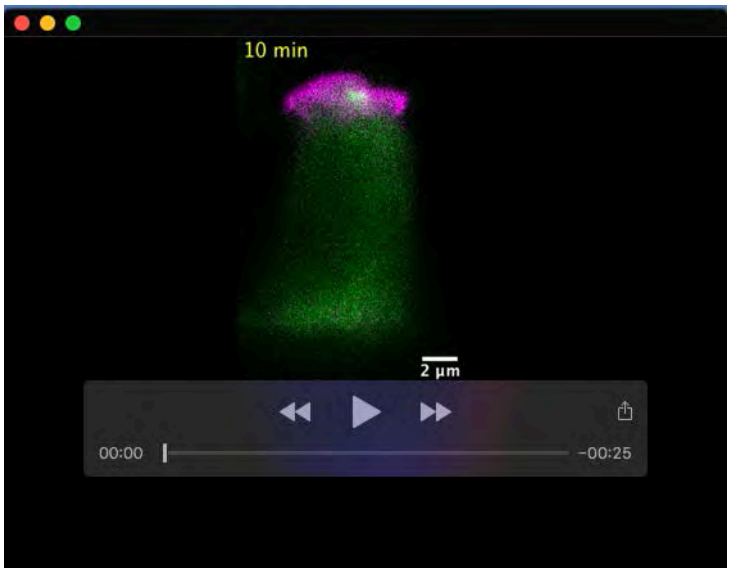

Movie 9. Live imaging of BB movements and Par3-RFP localization in a nonpolarizing FP cell. wt embryos mosaically expressing Centrin-GFP (green) and Par3-RFP (magenta). White arrows point at the BB at the beginning and end of movie. Images were taken every 5 minutes during the 17 s to 19 s stages time-frame. Lateral view. Corresponds to Fig4D.

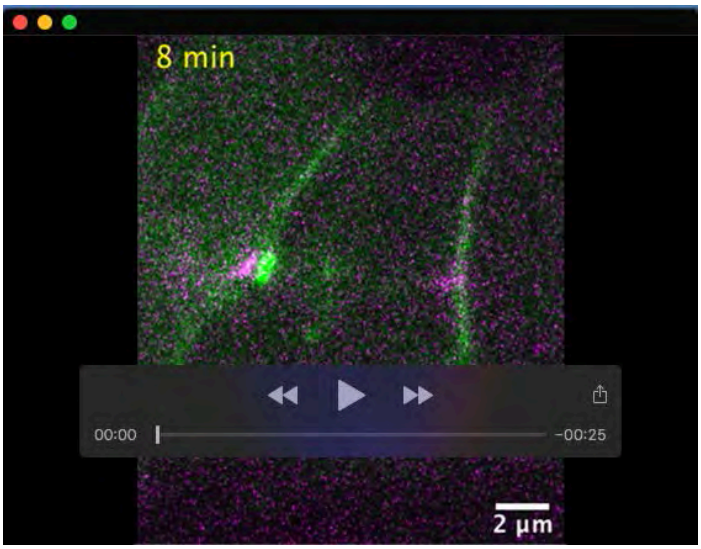

Movie 10. Live imaging of BB/Par3 patch contacts in an early-stage FP cell. wt embryo mosaically expressing Centrin-GFP, Membrane-GFP (green) and Par3-RFP (magenta). White arrows point at the BB at the beginning of the movie, when the BB is in contact with the anterior Par3 patch, at t=30 min when it makes a contact with the posterior Par3 patch and at the end of the movie. Images were taken every 2 min during the 4 s to 5 s stages time-frame. Dorsal view. Corresponds to the most anterior cell in Fig. 4E.

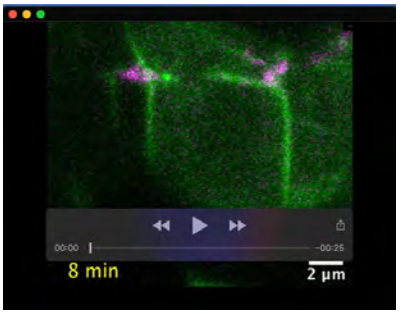

Movie 11. Live imaging of membrane digitations at Par3 patches in early stage FP cells. wt embryo mosaically expressing Centrin-GFP, Membrane-GFP (green) and Par3-RFP (magenta). White arrows point at the BB at the beginning and at the end of the movie. Yellow arrows at t=0 and t=68 min point at membrane digitations originating from the posterior and the anterior Par3 patches, respectively. Images were taken every 4 min during the 7 s to 8 s stages time-frame. Dorsal view. Corresponds to Fig4F.

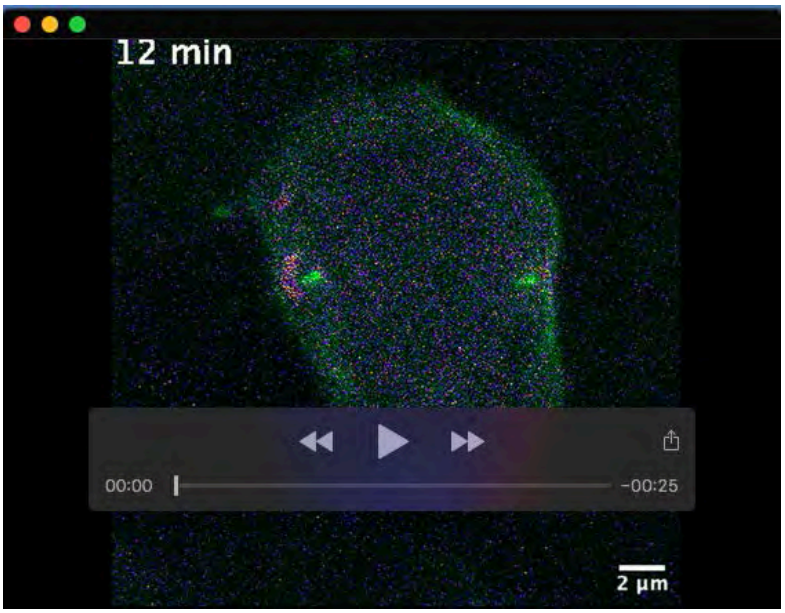

Movie 12. Live imaging of BB moving to Par3 patches after cytokinesis in dividing early stage FP cells. wt embryo mosaically expressing Centrin-GFP, Membrane-GFP (green) and Par3-RFP (Fire LUT, coding for fluorescence intensity). Yellow arrows at t=0 point at the posterior and the anterior Par3 patches which are present in FP cells in interphase. Yellow arrows at t=32min and t=36min point at BB/ Par3 patch contact in posterior and anterior daughter cells respectively. Images were taken every 4 min during the 5s to 6s stages. Dorsal view. Corresponds to Fig. S3B.

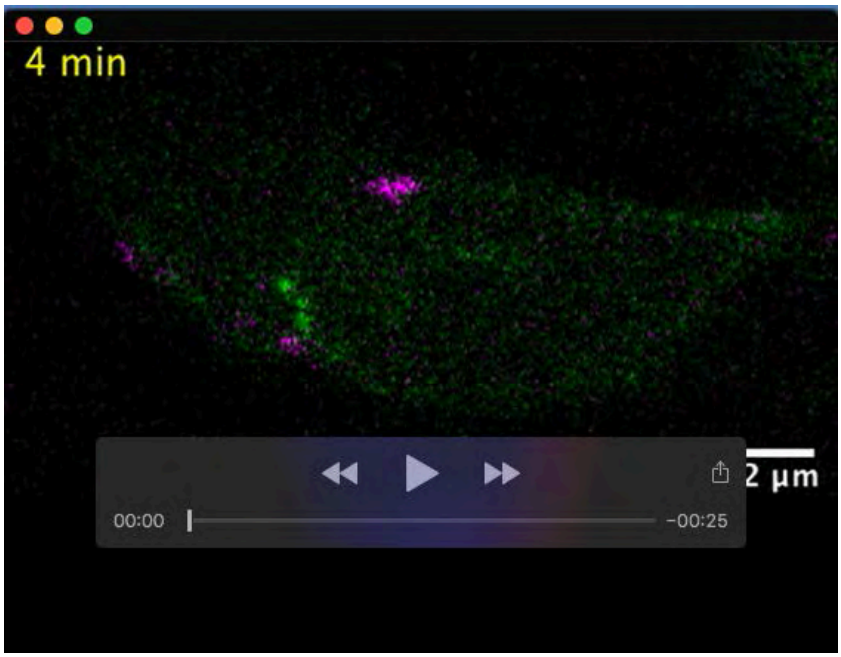

Movie 13. Live imaging of BB/lateral Par3 patch contacts in an early-stage FP cell of a *vangl2*$^{m209/m209}$ mutant. *vangl2*$^{m209/m209}$ embryo mosaically expressing Centrin-GFP, Membrane-GFP (green) and Par3-RFP (magenta). White arrows point at the BB at the beginning and at the end of the movie. Images were taken every 4 min during the 5 s to 6 s stages timeframe. Dorsal view. Corresponds to Fig7F, up.

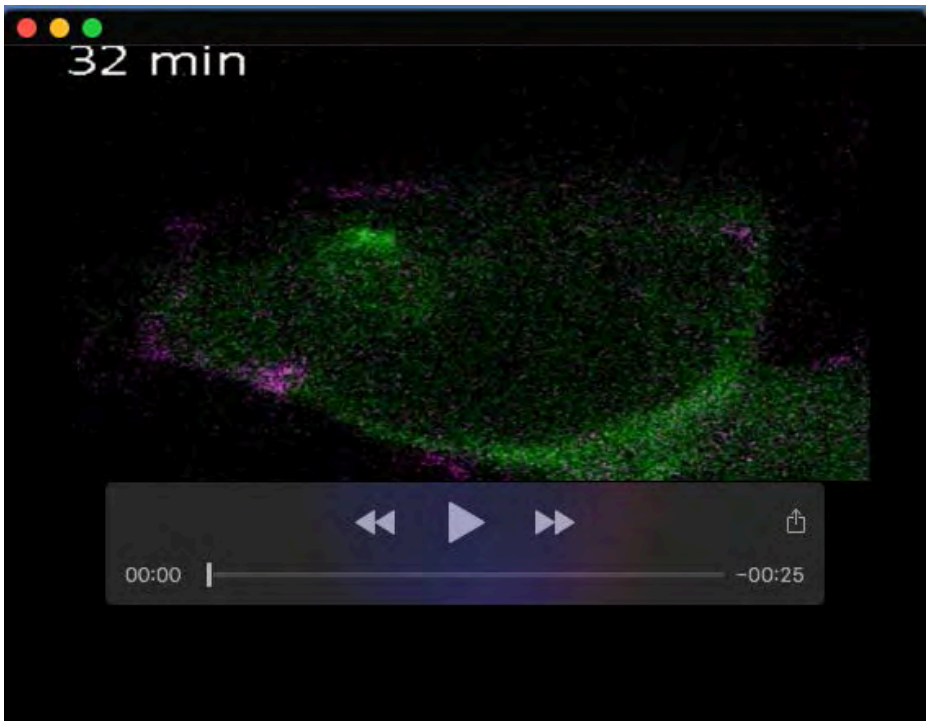

Movie 14. Live imaging of BB/lateral Par3 patch contacts in an early-stage FP cell of a *vangl2*$^{m209/m209}$ mutant. *vangl2*$^{m209/m209}$ embryo mosaically expressing Centrin-GFP, Membrane-GFP (green) and Par3-RFP (magenta). White arrows point at the BB at the beginning and at the end of the movie. Images were taken every 4 min during the 5 s to 6 s stages timeframe. Dorsal view. Corresponds to Fig. 7F, bottom.